

Synoptic-Scale Influence of the Saharan Air Layer on Tropical Cyclogenesis over the Eastern Atlantic

V. MOHAN KARYAMPUDI*

Department of Meteorology, University of Maryland, College Park, Maryland

HAROLD F. PIERCE⁺

Laboratory for Atmospheres, NASA Goddard Space Flight Center, Greenbelt, Maryland

(Manuscript received 4 January 2001, in final form 22 April 2002)

ABSTRACT

The formations of Hurricane Andrew, Tropical Storm Ernesto, and Hurricane Luis, which occurred, respectively, during the 1992, 1994, and 1995 hurricane seasons over the eastern Atlantic, have been investigated by utilizing the European Centre for Medium-Range Weather Forecasts (ECMWF) gridded data analyses. These cases were selected to illustrate the contrasting influences of the Saharan air layer (SAL) on tropical cyclogenesis.

Analyses results show that Tropical Storm Ernesto (1994) and Hurricane Luis (1995) formed from the merger of the low-level (925 hPa) and midlevel (700 hPa) vortices over the eastern Atlantic within the monsoon trough enhanced by surges in the trades. Midlevel vortices associated with each case appear to evolve from African wave troughs enhanced by cyclonic shear vorticity of the midtropospheric jet, which existed to the south of an SAL anticyclonic eddy as an elongated wind maximum. Vorticity budget calculations suggest that vortex stretching dominated the enhancement of low-level vortices, whereas positive vorticity advection (PVA) on the south and leading edge of the midlevel easterly jet (MLEJ) but ahead of the trough axis contributed to the enhancement of midlevel vortices for both cases. Persistent upper-level divergence associated with an anticyclonic circulation appears to have aided in the formation of Ernesto, whereas for Luis, no such prior forcing is evident.

Hurricane Andrew (1992), on the other hand, appears to form from a deep African wave vortex. Vortex stretching contributed to the development of low-level vortices. Although cyclonic shear vorticity to the south of the MLEJ is present in association with a deeper and wider SAL devoid of its characteristic anticyclonic eddy (unlike in Ernesto and Luis), the midlevel contribution from PVA on the south side of the jet to the maintenance of the midlevel vortex is found to be insignificant in Andrew due to negligible cross- (vorticity) contour flow to the south and ahead of the wave trough. However, the pre-Andrew growth was dominated by PVA at upper levels associated with easterly wave perturbations to the south of an anticyclonic circulation center but to the north of an upper-level easterly jet.

In at least two cases (i.e., Ernesto and Luis), the SAL directly contributed to the negative PV anomalies to the north of the MLEJ, which resulted in the sign reversal of the meridional gradient of potential vorticity (between 850- and 700-hPa levels), which satisfies the Charney and Stern criterion for barotropic and baroclinic instability across the midtropospheric jet over the eastern Atlantic. The baroclinic mechanism, proposed by Karyampudi and Carlson, is found to be valid in explaining some of the wave growth processes involved in the genesis of the same two cases. Based on these results, it is concluded that SAL had a positive influence on at least two cases [both (Ernesto and Luis) occurred in normal Sahel rainfall years], in contrast to a negative influence on Andrew, which occurred in an extremely dry year.

1. Introduction

Tropical cyclogenesis remains an enigma despite a large number of studies conducted over the past two decades not only because of the complex physical and

dynamical processes involved but also due to significant differences arising from oceanic (e.g., western Pacific), topographic (e.g., eastern Pacific), and differential heating (e.g., western Africa) influences. Many of the past studies dealt with genesis mechanisms such as air-sea interaction (Emanuel 1986, 1989), scale interaction (Holland 1995), vortex interaction (Simpson et al. 1997), ITCZ breakdown (Ferreira and Schubert 1997), monsoon confluence (Briegel and Frank 1997), environmental wind surge (Zehr 1992), and upper-tropospheric (Bosart and Bartlo 1991; Montgomery and Farrell 1993), topographic (Zehnder 1991), and easterly

* Current affiliation: SAIC/NCEP/NOAA, Camp Springs, Maryland.

⁺ Additional affiliation: Science Systems and Applications, Inc., Lanham, Maryland.

Corresponding author address: Dr. V. Mohan Karyampudi, NOAA/NCEP, 5200 Auth Rd., Camp Springs, MD 20746.
E-mail: Mohan.Karyampudi@noaa.gov

wave (Molinari et al. 2000) influences. Although a majority of these studies have focused on tropical cyclone formation over the tropical Pacific, a detailed study is yet to be carried out to understand the genesis mechanisms over the eastern Atlantic–western Africa region, where some of the most intense Atlantic hurricanes that cause much of the destruction over the East Coast and Caribbean Islands originate from easterly waves (Landsea and Gray 1992).

Although tropical cyclogenesis involves both dynamical and thermodynamical processes over many spatial and temporal scales, much progress has been made in understanding genesis mechanisms with the data collected in the field programs such as the Tropical Experiment in Mexico [TEXMEX; (e.g., Biester and Emanuel 1997; Farfan and Zehnder 1997)], the Tropical Cyclone Motion experiment of 1993 (TCM-93; e.g., Harr et al. 1996), and the Tropical Ocean Global Atmosphere Coupled Ocean–Atmosphere Research Experiment (TOGA COARE; e.g., Simpson et al. 1997). Studies by Zehr (1992), Simpson et al. (1997), and Gray (1998) suggest that tropical cyclogenesis consists of at least two stages. In the first, or preformation, stage, the large-scale dynamical processes dominate as the low-level vorticity maximum increases prior to the formation of a finite-amplitude vortex at the surface; whereas in the second, or formation, stage, both dynamical and thermodynamical processes dominate through the scale interaction of mesoscale vortices embedded within the synoptic to subsynoptic-scale disturbances leading to eye formation and decrease in central pressure. The recent synoptic-scale studies of tropical cyclogenesis such as those by Molinari et al. (2000) and Bracken and Bosart (2000) can be classified under stage 1. [For a general summary of large-scale cyclogenesis processes, the reader is referred to the recent studies by Molinari et al. (2000) and Bracken and Bosart (2000).] Stage 2 processes, on the other hand, involve interaction of mesoscale vortices such as those described by Ritchie and Holland (1993) and Simpson et al. (1997). These mesoscale-scale interaction processes cannot be addressed here due to the large-scale nature of the European Centre for Medium-Range Weather Forecasts (ECMWF) analyses. As such, the present study deals with stage 1 processes, and in some ways is similar to that of Molinari et al. (2000) in relating the dynamical processes involved in the development of the preformation stage vortex associated with African waves.

It is well known that the occasional African disturbances that develop into Atlantic hurricanes are often referred to as “Cape Verde” hurricanes since their first surface signatures often appear as vortices within the equatorial trough region off the coast of West Africa near the Cape Verde Islands (Simpson and Riehl 1981). Characteristics of the African disturbances, which are similar to the classical easterly wave structure proposed by Riehl (1954), have been studied extensively by Carlson (1969a,b), Burpee (1972, 1975), and Reed et al.

(1977). They found that these disturbances cross the West African coastline typically between early June and October at a frequency of 3–4 days with wavelengths of 2000–3000 km and phase speeds of 6°–7° (8 m s^{-1}) longitude per day. Burpee (1972) was among the first to claim that easterly wave perturbations derive their energy from strong vertical and horizontal shears of the mean zonal wind. He found that the mean potential vorticity gradient across the midlevel easterly jet (MLEJ) vanishes over North Africa ($\sim 5^\circ\text{E}$), which appears to satisfy the combined barotropic–baroclinic instability criterion given by Charney and Stern (1962) for an internal jet. Later Reed et al. (1977), using Global Atmosphere Research Program (GARP) Atlantic Tropical Experiment (GATE) data, verified that African wave disturbances indeed satisfy the necessary condition for barotropic instability of the zonal flow as they found a region in which the gradient reverses in the vicinity of the MLEJ.

The MLEJ jet dynamics was further investigated by Schubert et al. (1991), who emphasized the role of ITCZ convection in providing a positive potential vorticity (PV) anomaly to the south of the jet and, hence, its role as an energy source for African waves. But Thorncroft and Blackburn (1999) clearly showed that thermal-low heating over the Sahara to the north of the jet [i.e., the PV destruction within the deep mixed layer, referred to in this study as the Saharan air layer (SAL)] is crucial in maintaining the jet as well as in setting up the negative meridional PV gradients that characterize the observed MLEJ structure. The PV destruction within the SAL has previously been noted by Marks (1980) in his study on the organization of mesoscale cloud lines to the south of the SAL boundary.

The SAL, which becomes an elevated mixed layer over the Atlantic, transports large-scale Saharan dust outbreaks across the tropical Atlantic during the summer months (Carlson and Prospero 1972). These dust outbreaks (2000–3000 km), which are confined predominantly within the ridge region of passing easterly wave disturbances, occur with a periodicity of 5–7 days (Prospero and Carlson 1981). The SAL yields a warm anomaly at 850 hPa to the north of the MLEJ as depicted in the mean structure of African waves by Reed et al. (1977), who attribute the strong temperature contrast to the warm Saharan air (i.e., the SAL) to the north and the cooler air overlying the ocean waters to the south (see their Fig. 2c). The essential role of the SAL in the maintenance of the MLEJ (through thermal wind balance) downstream of West Africa including the influence of the MLEJ on the growth of a wave disturbance that subsequently developed into a tropical cyclone has been studied by Karyampudi and Carlson (1988). They showed that an elongated MLEJ, located between the wave trough axis and the downstream ridge axis at the southern edge of a Saharan dust outbreak is favorable for wave growth mainly due to the baroclinic conversion of eddy available potential energy to eddy kinetic en-

ergy, in contrast to the barotropic energy conversion emphasized by Norquist et al. (1977) for the eastern Atlantic region. These results were found to be consistent with those of Spencer (1981), who noted the important role played by MLEJ at the leading edge of the SAL in the development of an African wave (i.e., a tropical depression) over the eastern Atlantic.

The growth of the wave disturbances due to the interaction between the Saharan dust layer and the African waves has been envisaged by Karyampudi and Carlson, which they referred to as the baroclinic mechanism, as follows: (i) a Saharan dust outbreak (i.e., the SAL) following a wave disturbance is favorable for imposing baroclinity along the leading and southern edges of the SAL front; (ii) the MLEJ is maintained along the SAL front by the horizontal temperature gradient imposed by the SAL; (iii) cyclonic shear vorticity at 700 hPa on the south side of the jet near the trough axis is compatible with low-level convergence and upward motion, particularly in the region of the left exit quadrant of the jet, where there is positive vorticity advection increasing with height below 700 hPa; and (iv) ascent in the presence of conditional instability initiates vigorous convection in the wave disturbance, which leads to intensification of the wave disturbance through conditional instability of the second kind (CISK).¹ Karyampudi and Carlson further suggested that large-scale heavy dust outbreaks, on the other hand, are not conducive for tropical cyclone formation. This is due to the equatorward compensating subsidence induced by the rising motion within the dust plume to the north (resulting from dust heating), which suppresses disturbance growth as it counters the Hadley circulation, at least in the low to midlevels.

The presence of SAL in the vicinity of tropical storm formation over the eastern Atlantic has been noted in a few other studies (e.g., Douglas 1977; Marks 1980; Karyampudi et al. 1999). In spite of the common occurrence of a developing vortex to the south of the MLEJ² that is maintained by the SAL anticyclonic eddy, the exact dynamical relationship between the Saharan dust layer (i.e., the SAL) and tropical storm formation is yet to be determined. Therefore, it is the purpose of this study to clarify this relationship in the context of applying the baroclinic mechanism to large-scale tropical cyclogenesis over the eastern Atlantic using a few cases that occurred during 1992, 1994, and 1995. A secondary objective of this study is to contrast the differences in SAL influences on cyclogenesis in dry (1992) and normal (1994 and 1995) Sahel rainfall years since it is known that drought conditions over the Sahel increase

the intensity and frequency of dust outbreaks (Prospero and Nees 1986; Swap et al. 1996). Intense and widespread dust within the SAL, on the other hand, adversely impacts the development of African waves since equatorward subsidence induced by the SAL is found to inhibit deep convection (on the equator side of the middle-level jet) in conjunction with less perturbed zonal flow (Randall et al. 1984; Karyampudi and Carlson 1988).

In the following section, ECMWF data and the analysis methodology (involving diagnostic variables and vorticity budget) are outlined. Detailed analyses of the genesis of Tropical Storm (TS) Ernesto including two other cases (Hurricanes Luis and Andrew) are provided in section 3 to help understand the contrasting influences of the SAL on genesis processes over the eastern Atlantic. In section 4, the combined barotropic and baroclinic instability is examined in the context of its applicability to tropical cyclogenesis over the eastern Atlantic. Finally, a summary and discussion is presented in section 5.

2. Data and analysis methodology

a. Genesis definition

The necessary conditions for tropical cyclone formation were enumerated by Gray (1968) and Riehl (1979). McBride and Zehr (1981) found that the disturbances that developed into tropical cyclones are associated with high values of low-level relative vorticity (ζ) and upper-level divergence and negligible vertical shear near the system center. Gray (1975) and McBride (1981) further argue that the thermodynamic parameters such as sea surface temperatures, conditional instability, and large values of relative humidity exist most of the time in the tropical atmosphere as they remain above threshold values necessary for tropical cyclone development. Among the six seasonally averaged parameters, Gray (1998) emphasizes the important role of dynamical parameters such as low-level relative vorticity and small vertical wind shear when the synoptic flow is perturbed above its regional climatological values. In a review, Frank (1987) further underscores that the necessary conditions required to form a tropical cyclone are strongly related to the dynamic parameters specified by the wind field rather than the thermodynamic fields.

In the present study, tropical cyclone genesis is interpreted, following Frank (1987), as the state of transition from a disturbance to a depression involving the initial formation of a rotational circulation with a scale of a few hundred kilometers. *Genesis is defined herein as the stage of occurrence when low-level closed circulation first appears, and not necessarily when the disturbance is declared a tropical depression.*

b. ECMWF data

Since the emphasis of this study is on large-scale (i.e., the first stage of) tropical cyclogenesis mechanisms, it

¹ Because CISK is controversial, a revised baroclinic mechanism is proposed in section 5, which excludes CISK based on the results of this study.

² Forecasters at the Tropical Prediction Center frequently note that tropical storm formation in the eastern Atlantic region is often preceded by the middle-level jet within a wave disturbance.

is assumed that coarse-grid datasets such as the ECMWF analyses are adequate enough to represent the genesis processes. Previously, Karyampudi and Carlson (1988) and Zehr (1992) have shown, respectively, that coarse-grid horizontal resolution of 2° – 2.5° is sufficient to resolve easterly wave and pretropical storm disturbances. Other investigators have also used ECMWF gridded analyses for their reliability to accurately analyze tropical systems over data-sparse oceanic regions (e.g., Reed et al. 1988; Lau and Lau 1990; Molinari et al. 2000). Therefore, ECMWF gridded data, available at 2.5° latitude \times 2.5° longitude resolution on 13 mandatory levels (i.e., at 1000, 925, 850, 700, 500, 400, 300, 250, 200, 150, 100, 70, and 50 hPa), from National Center for Atmospheric Research (NCAR) data archives have been utilized at every 12 h for further diagnostic calculations by converting the data into General Meteorological Package (GEMPAK; desJardins and Petersen 1983) format. (Note that ECMWF gridded data at finer spatial resolution were not readily available for this study.) In order to obtain confidence in the ECMWF data, however, the analyses were checked for qualitative accuracy by comparing them with observations such as soundings and satellite imagery.³ Vertical time sections of winds, temperature, and relative humidity extracted from the ECMWF data at two locations, Sal Island (Cape Verde Islands) and Dakar (Senegal), were compared against time sections constructed from sounding data at the same locations for two cases (i.e., TS Ernesto and Hurricane Andrew). These sounding comparisons showed that the ECMWF data were able to reproduce well not only the time of passage of these wave disturbances and the SAL but also their vertical structure (not shown). From these qualitative comparisons, it has been determined that ECMWF data are sufficiently accurate in portraying the structure and passage of important synoptic-scale features such as easterly waves, the SAL, and low-level monsoon features, at least in locations where there is adequate data such as over the western Africa and the eastern Atlantic (i.e., in the vicinity of the Cape Verde Islands) regions, despite the fact that there might be some differences in the quality of the analyses between 1992 and 1994/1995, perhaps due to different models and analysis methods.

The selection of the three [i.e., Hurricane Andrew (1992), TS Ernesto (1994), and Hurricane Luis (1995)] cases was based on the following reasons: (i) the TS Ernesto precursor evolved during the Lidar in-Space Technology Experiment (LITE) (10–19 September 1994), and these lidar data were previously analyzed in

detail by Karyampudi et al. (1999); (ii) the desire to highlight contrasting influences of the SAL in dry [1992 was known to be the driest over the west Sahel (C. Landsea 2001, personal communication) with only one storm forming over the eastern Atlantic] and normal [1995 was known to be a prolific year with a near-record-breaking number of tropical cyclones, including the most intense hurricanes originating from African waves (Lawrence et al. 1998)] Sahel rainfall years; and (iii) their proximity to the Cape Verde Islands (i.e., the region of interest in this study) when each of these systems developed into a tropical depression.

Diagnostic variables such as divergence, vorticity, potential temperature, meridional gradients of potential temperature and potential vorticity, and vertical and horizontal gradients of the u component of the wind (i.e., $\delta u / \delta p$ and $-\delta u / \delta y$), including vorticity budgets, were calculated for the three tropical cyclogenesis cases (at both 0000 and 1200 UTC synoptic times). Vorticity budgets were evaluated by applying the following equation:

$$\begin{aligned} \frac{\partial}{\partial t}(\zeta + f) = & -\mathbf{V} \cdot \nabla_H(\zeta + f) - \omega \frac{\partial \zeta}{\partial p} - (\zeta + f) \nabla_H \cdot \mathbf{V} \\ & + \left(\frac{\partial \omega}{\partial y} \frac{\partial u}{\partial p} - \frac{\partial \omega}{\partial x} \frac{\partial v}{\partial p} \right) + F_r. \end{aligned} \quad (1)$$

The first two terms on the right-hand side, respectively, represent the horizontal and vertical vorticity advections, whereas the next two terms represent the stretching and tilting terms, respectively. The last term, which represents the frictional term, however, was neglected since it is assumed to be unimportant at the initial stage of vortex development over the ocean. The vorticity tendency term is the sum of all four terms. All the terms were evaluated at each synoptic time (i.e., both at 0000 and 1200 UTC) during the period prior to and after the genesis time of occurrence. In order to obtain spatially averaged quantities, vorticity budget terms including other variables such as wind speed, divergence, and relative vorticity have been averaged over nine grid points (i.e., over a 5° lat \times 5° lon grid box) centered at the location where the low-level circulation in the wind field (i.e., at 925 hPa) first appeared according to the definition given in section 2a. In addition, daily genesis potential (DGP), defined by McBride and Zehr (1981) as the mean relative vorticity difference between 900 and 200 hPa to distinguish the differences between developing and nondeveloping tropical disturbances, has also been evaluated at the genesis time (note that the 925-hPa level was substituted for 900-hPa level as ECMWF data at this level were not available). To obtain SAL width and height estimates, SAL widths were qualitatively estimated from the north–south potential temperature cross sections taken across the disturbance genesis locations for each of the three cases, whereas the SAL tops were estimated from the time section plots of observed soundings taken at the Cape Verde Islands,

³ Karyampudi et al. (1999) have shown that the ECMWF analyses were able to capture large-scale features such as the African waves and the Saharan dust layer eddy at 700 mb (i.e., the level at which the easterly waves exhibit their maximum amplitude) adequately well by comparing the analyses against visible satellite imagery, lidar, and dropwindsonde data for the TS Ernesto case (i.e., 16–19 September 1994).

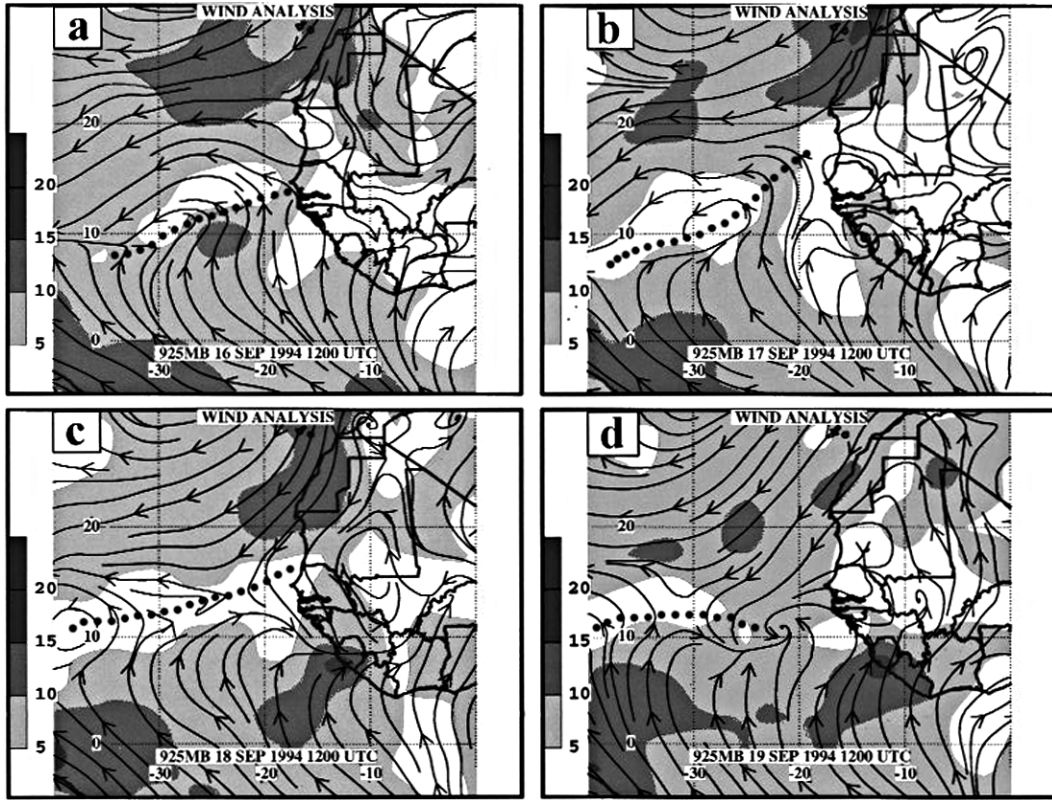


FIG. 1. The 925-hPa wind analyses from ECMWF data at 1200 UTC on (a) 16 Sep, (b) 17 Sep, (c) 18 Sep, and (d) 19 Sep 1994. (Contour lines are streamlines; wind speeds are shaded; shading bar is given next to each panel at 5 m s⁻¹ intervals). The dotted line indicates the monsoon shear line described in the text.

which are located to the north of the genesis location of all three cases. (Note that the observed soundings were used in lieu of ECMWF data due to poor vertical resolution of the ECMWF analysis between 500 and 700 hPa.) Furthermore, weekly averages of winds and potential temperature (centered at the genesis time of occurrence) were obtained to evaluate the meridional gradient of PV across the midtropospheric jet. However, mean PV gradient calculations were made on pressure surfaces in a manner similar to that of Molinari et al. (2000), who used absolute vorticity (ζ_a) gradients instead of PV gradients.

3. Synoptic-scale analyses of cyclogenesis cases

Analyses of the following three cases (i.e., TS Ernesto, and Hurricanes Luis, and Andrew) are presented in this section to illustrate the contrasting dynamical influences of the SAL on cyclogenesis over the eastern Atlantic.

a. TS Ernesto (1994)

Ernesto developed from a tropical wave that emerged from the coast of West Africa on 18 September as it appeared over the eastern tropical Atlantic and attained

tropical depression status at 1800 UTC 21 September when the system was located about 925 km southwest of the Cape Verde Islands (Avila and Rappaport 1996). The life of Ernesto was rather brief as it weakened rapidly after reaching a peak intensity of 997 hPa (50-kt maximum winds) at 0000 UTC 23 September at 13.1°N, 30.4°W and encountered an unfavorable environment as it moved northward. It was only one of two storms that formed over the eastern Atlantic in 1994.

The evolution of Ernesto's precursor can be seen in the 925-hPa streamline analysis in Fig. 1, for 16–19 September 1994, which clearly depicts the formation of a cyclonic circulation at about 10°N, 23°W within the monsoon confluence line by 1200 UTC 19 September (Fig. 1d). The corresponding mean sea level pressure (MSLP) charts (not shown) reveal the formation of a closed isobar of 1012 hPa near the cyclonic circulation center embedded within the broad monsoon. Further evidence that this circulation is indeed the precursor of Ernesto can be gleaned from the inspection of the visible satellite imagery shown by Karyampudi et al. (1999). (See their Fig. 4, which clearly depicts cyclonically curved cloud bands in the vicinity of this wind circulation and sea level pressure center.) One should note, however, that the location of the analyzed disturbance

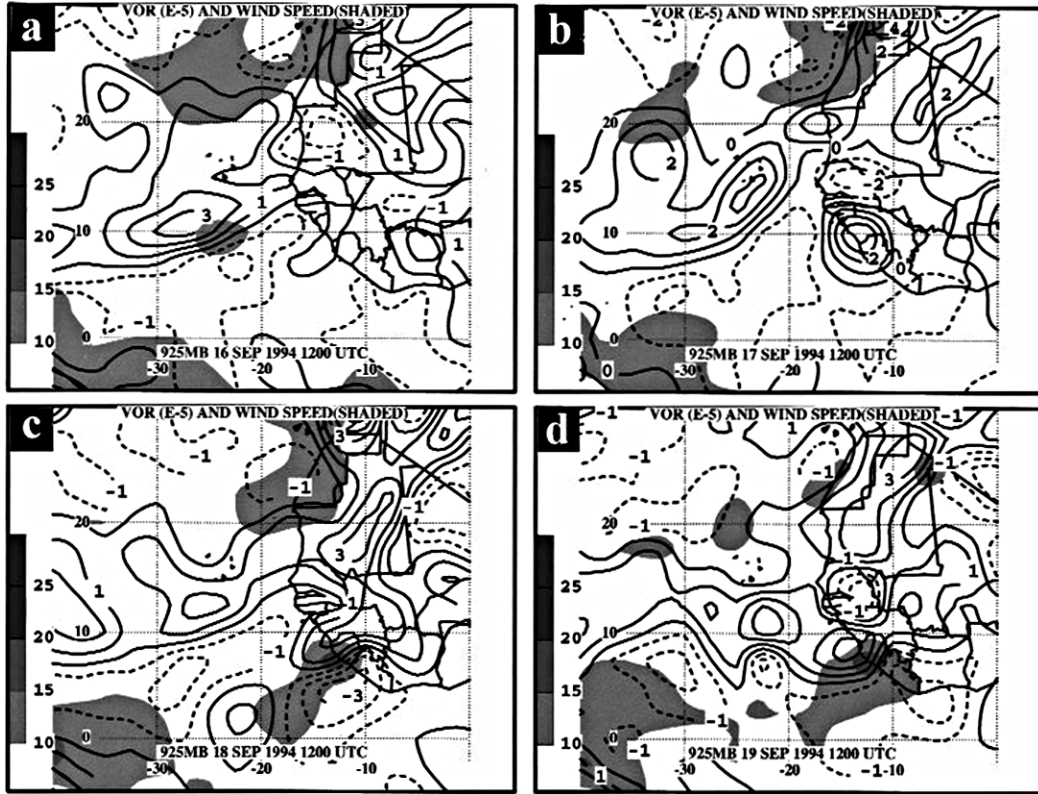


FIG. 2. The 925-hPa relative vorticity (ζ) and wind speed analyses from ECMWF data at 1200 UTC on (a) 16 Sep, (b) 17 Sep, (c) 18 Sep, and (d) 19 Sep 1994. Contour lines are ζ (negative values are dashed: $1 \times 10^{-5} \text{ s}^{-1}$); gray shades represent wind speeds $>10 \text{ m s}^{-1}$ at 5 m s^{-1} intervals.

lagged the cloud circulation pattern visible in the satellite imagery by a few degrees.

The monsoon shearline, which delineates the northeasterlies on the poleward side and southwesterlies on the equatorward side, is a semipermanent feature during summer over the western Africa–eastern Atlantic region (Sadler 1975). It coincides with the monsoon trough and can be seen in the 925-hPa streamline analysis (see the dotted line in Fig. 1). The synoptic-scale variability of the shear line in the summer months is mostly due to vortices traveling westward in the monsoon trough (Sadler 1975). Accordingly, the shear line, which is oriented in a southwest-to-northeast direction at 1200 UTC 17 September (Fig. 1b), progresses southward and becomes oriented parallel and north of the confluence line by the time the cyclonic circulation appears near 11°N , 22°W at 1200 UTC 19 September (Fig. 1d). The 925-hPa divergence field (not shown) indicates that this shear line overlapped the confluence line as a broad area of maximum convergence extended along the confluence line, particularly at 1200 UTC 19 September. These features extended to the 850-hPa level as the wind field at 850 hPa (not shown) clearly depicted the southward migration of the shear line as well as the formation of low-level cyclonic circulation associated with the Ernesto precursor.

The southward migration of the shear line as well as the evolution of the Ernesto precursor can be viewed more clearly in the 925-hPa relative vorticity (ζ) and wind speed chart (Fig. 2). Figure 2 shows the southward displacement of the maximum relative vorticity axis associated with the monsoon trough, which is located parallel to the shear line, from a southwest–northeast orientation to an east–west orientation. Furthermore, this figure (in conjunction with high temporal resolution analyses at every 12 h; not shown) indicates that the vorticity maximum ($\zeta > 2 \times 10^{-5} \text{ s}^{-1}$ located at $\sim 11^\circ\text{N}$, 22.5°W at 1200 UTC 19 September in Fig. 2d) associated with the Ernesto precursor appears to originate from the same vorticity maximum that was located to the west and northwest earlier between 16 and 18 September (i.e., the maximum ζ center located around 11°N , 27°W at 1200 UTC 16 September; see Fig. 2a). The vorticity source appears to be associated with the remnant of an easterly wave trough axis that is enhanced by the southwesterly monsoon surge to the east of the trough axis as can be seen in Fig. 1a (i.e., the wind maximum $>10 \text{ m s}^{-1}$ to the south of the shear line around 10°N , 25°W). [Note that the strong southwesterly winds can be classified as a monsoon surge since they appear to result from the pressure gradient set up by the subtropical high pressure region to the south of the equa-

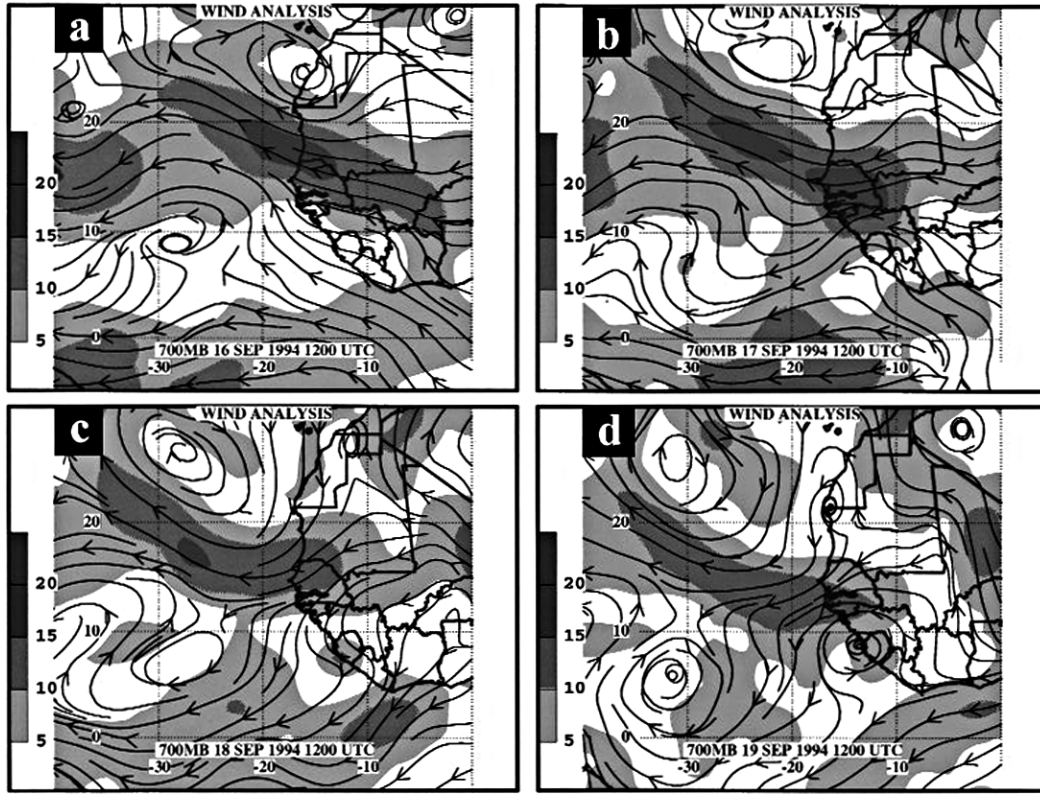


FIG. 3. Same as in Fig. 1 except at 700 hPa.

tor and lower pressures within the monsoon trough to the north behind the leading wave trough (i.e., on the east side of the wave trough axis) (not shown).]

It is well known that the 700-hPa level typically represents the MLEJ and African wave structure (Reed et al. 1977). The wind field at this level corresponding to the same period (Fig. 3) shows an elongated wind maximum ($>10 \text{ m s}^{-1}$), which can be referred to as the MLEJ, oriented in a west-northwest to east-southeast direction between the upstream trough axis (located roughly along 29°W with a closed circulation centered at about 9°N , 28°W in Fig. 3a) and the downstream ridge region (i.e., the ridge axis along 15°W). Previously, Karyampudi et al. (1999) have presented evidence based on lidar data that this elongated MLEJ was present on the southern edge of a Saharan dust outbreak (i.e., the SAL anticyclonic eddy centered at about 24°N , 16°W in Fig. 3a) but embedded within a broad-scale high pressure system (i.e., the anticyclonic circulation to the north of 20°N in Figs. 3a–d). This jet arises as a consequence of thermal wind arising from the warm and dry SAL to the north and the cool equatorial moist air to the south, which can be seen in the 850-hPa⁴ meridional temper-

ature gradient ($\delta\theta/\delta y$) field depicted in Fig. 4. It is clear from this figure that the positive temperature gradient, which is coincident with the MLEJ (shaded in gray) throughout the 16–19 September period and located at the southern edge of the SAL, possesses maximum values of the order of $\sim 10 \times 10^{-6} \text{ K m}^{-1}$. This is equivalent to $1 \text{ K (100 km)}^{-1}$ along the southern and leading edge of the SAL, which is compatible with the temperature gradient reported by Karyampudi and Carlson (1988). (The MLEJ speed of 16 m s^{-1} is in approximate thermal wind balance with the temperature gradient of $10 \times 10^{-6} \text{ K m}^{-1}$.) Furthermore, this midtropospheric jet is associated with not only horizontal shears but also maximum vertical wind shears of the order of 16 m s^{-1} between 1000 and 700 hPa (not shown).

Most importantly Fig. 3 also shows the evolution of cyclonic flow associated with the north–south-oriented trailing wave trough axis (i.e., the trough axis along 12°W to the south of the trailing wind maximum in Fig. 3b), as it amplifies and reorients in a northwesterly–southeasterly direction along $\sim 10^\circ\text{N}$ to the south of the elongated MLEJ in Figs. 3c and 3d. Note that this cyclonic flow is associated with cross-(isotach) contour flow, particularly in Fig. 3d, as can be noted from the abrupt southward turn of the stream lines to the south of the elongated MLEJ and across the trough axis (between 15° and 30°W). The cross-contour flow in Fig. 3d also coincides with the low-level cyclonic circulation in Fig. 1d.

⁴ Note that, previously, Karyampudi and Carlson (1988) have shown that the 850-hPa level captures the north–south temperature gradient over the eastern Atlantic region as a result of the warm SAL base being elevated to this level after the SAL leaves the West African coastline.

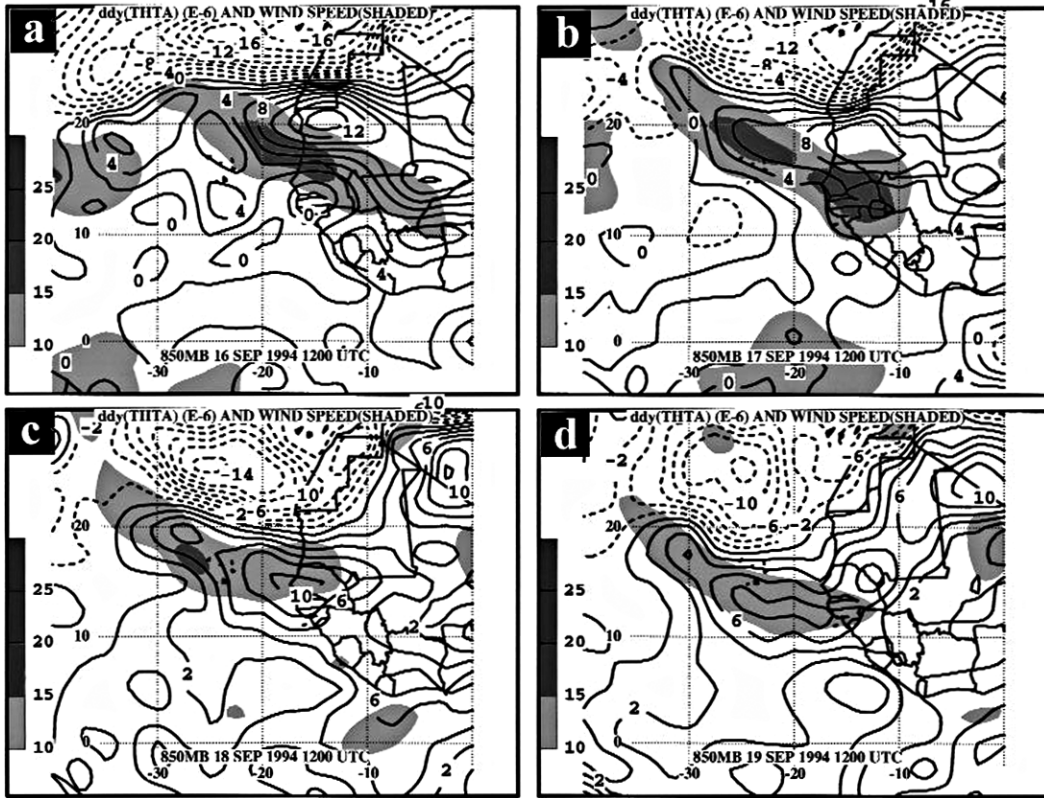


FIG. 4. The 850-hPa meridional potential temperature gradient (θ_y) and wind speed analyses from ECMWF data at 1200 UTC on (a) 16 Sep, (b) 17 Sep, (c) 18 Sep, and (d) 19 Sep 1994. Contours are θ_y (negative values are dashed: $2 \times 10^{-6} \text{ K m}^{-1}$); gray shades denote wind speeds $> 10 \text{ m s}^{-1}$ at 5 m s^{-1} intervals.

One of the essential features of the baroclinic mechanism is the presence of cyclonic shear vorticity (i.e., $-\delta u / \delta y > 0$) to the south of the MLEJ (refer to section 1), which clearly exists in this case as can be seen in Fig. 5. This figure clearly depicts the north–south cyclonic shear vorticity component of ζ collocated with the cyclonic shear on the south side of MLEJ (shaded in gray) at 700 hPa, which comprises a large portion of the positive relative vorticity (not shown). By inspecting Figs. 3 and 5, one can infer the likely occurrence of positive vorticity advection to the south and west of the MLEJ, particularly during 1200 UTC 18 September and 1200 UTC 19 September (i.e., ahead of the trough axis located between 10°N , 18°W and 12°N , 25°W), arising from the cross-contour flow mentioned earlier. (Note that the presence of this cyclonic shear vorticity to the south of the jet including the likely occurrence of positive vorticity advection arising from the cross-contour flow is essential to the role of positive vorticity advection on the wave growth as hypothesized by Karyampudi and Carlson; this is discussed further later.) The plausible role of positive vorticity advection (PVA) on wave growth can be gleaned from Fig. 5, which shows the increase of the maximum shear vorticity center ($> 2 \times 10^{-5} \text{ s}^{-1}$), located across the West African coastline on the south side of the MLEJ ($> 15 \text{ m s}^{-1}$) at 1200

UTC 17 September (see Fig. 5b), to $> 3 \times 10^{-5} \text{ s}^{-1}$ (centered around 12°N , 22.5°W) by 1200 UTC 19 September (Fig. 5d) as it migrated westward along with the wind maximum and became a well-defined positive vorticity center (PVC). Interestingly, this 700-hPa PVC, which occurred to the south of the SAL anticyclonic eddy (refer to Fig. 3), is juxtaposed with the low-level (925 hPa) vorticity center described earlier (i.e., the center that migrated from northwest of the genesis location) to evolve into a deep lower-tropospheric vortex that appears to extend from the surface to at least the 700-hPa level as described below.

In order to examine the vertical structure and understand the large-scale vortex formation processes, spatially averaged wind speed, relative vorticity, divergence, and vorticity budget terms (refer to section 2b for details) at 10°N , 22.5°W (i.e., the surface vortex location at 1200 UTC 19 September) are plotted in vertical time cross sections between 1200 UTC 16 September and 1200 UTC 22 September. Figures 6a–c show the relative vorticity, divergence, and wind speed plots, which exhibit the following important features. (i) The vorticity maximum ($> 14 \times 10^{-6} \text{ s}^{-1}$) associated with the precursor appears first at low levels (i.e., at 925 hPa) around 1200 UTC 19 September; note that the middle-level vorticity maximum ($> 18 \times 10^{-6} \text{ s}^{-1}$ centered at

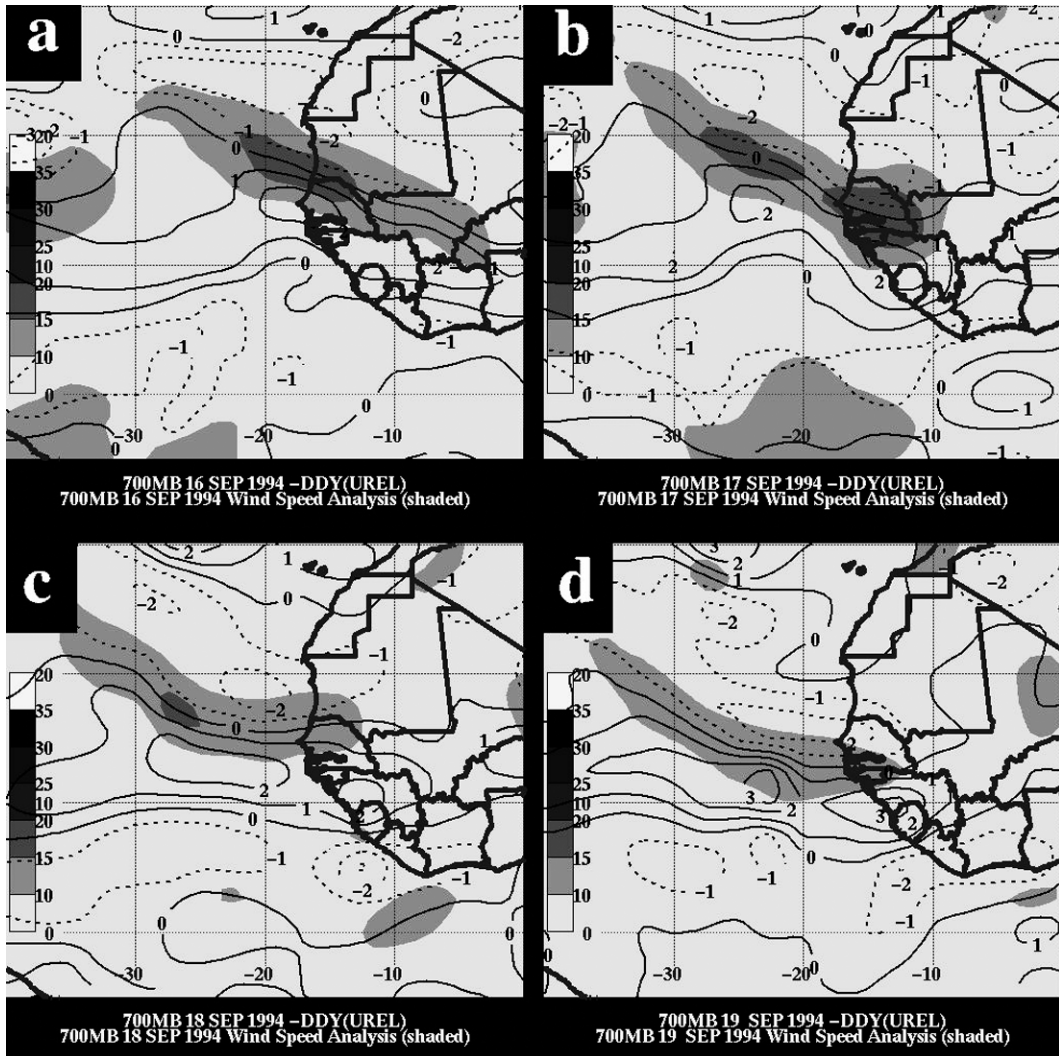


FIG. 5. The 700-hPa meridional wind shear component of relative vorticity $\zeta_y (-\delta u / \delta y)$ and wind speed analyses from ECMWF data at 1200 UTC on (a) 16 Sep, (b) 17 Sep, (c) 18 Sep, and (d) 19 Sep 1994. Contour lines are ζ_y (negative values are dashed) at $2 \times 10^{-5} \text{ s}^{-1}$; gray shading represents wind speeds at 5 m s^{-1} intervals.

700 hPa) appears slightly later, beginning at 0000 UTC 20 September (Fig. 6a). (ii) The low-level vorticity center coincides with the low-level convergence maximum at 0000 UTC on 20 September (cf. Figs. 6a and 6c). (iii) The midlevel relative vorticity core, which resides longer at 700 hPa, tilts eastward with height (assuming that the easterly wave disturbance is propagating from east to west). (iv) The 700-hPa vorticity maximum coincides with the MLEJ location and occurrence (cf. Figs. 6a and 6b). (v) An upper-level outflow jet at 200 hPa ($>10 \text{ m s}^{-1}$; Fig. 6b), perhaps associated with deep convection, occurs at about the genesis time; the ζ field shows a broad region of anticyclonic vorticity centered between 150 and 200 hPa beginning on 18 September as can be seen in Fig. 6a [note that an inspection of the 200-hPa level streamline and divergence fields indicates that the low- to midlevel vortex formed underneath an

east–west-oriented ridge axis that separated a strong westerly flow to the north and weak easterly flow to the south (not shown). Such a feature was shown to be necessary in the formation of tropical cyclones over the eastern Atlantic by Bracken and Bosart (2000)]. (vi) The divergence time section (Fig. 6c) shows a broad upper-level divergence centered at 300 hPa on 19 September at about the time the upper-level jet appears (Fig. 6b). All these features suggest that the low-level (925 hPa) vortex occurred first in a region dominated by an upper-level anticyclonic region, whereas the middle-level (700 hPa) vortex associated with the MLEJ propagated into this region later to become a deep vortex with an apparent eastward vertical tilt with height.

Vorticity budget time cross section plots are shown in Fig. 7 not only to examine the vortex generation mechanisms but also to verify whether PVA at 700 hPa

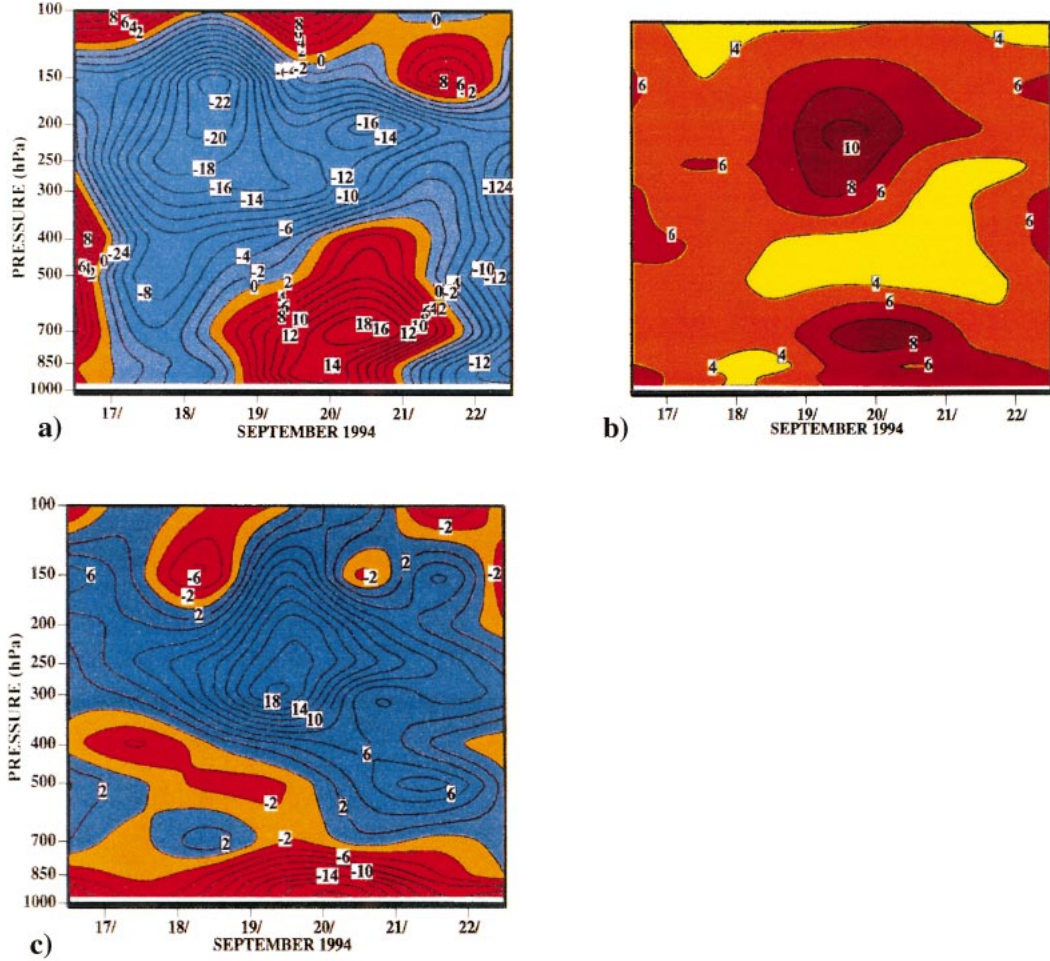


FIG. 6. Area-averaged (over 5° lat \times 5° lon grid box) vertical time sections for 16–22 Sep 1994 at the TS Ernesto genesis location (10°N , 22.5°W): (a) ζ [contour (positive: red; negative: blue) at $2 \times 10^{-6} \text{ s}^{-1}$], (b) wind speed (contour lines: 2 m s^{-1}), and (c) divergence (div) (contour lines: $2 \times 10^{-6} \text{ s}^{-1}$). The numbers along the x axis represent the dates at 0000 UTC.

exists to the south of the MLEJ but ahead of the wave trough axis as inferred from the cross-contour flow mentioned earlier. These vorticity budget panels show the following highlights. (i) The midlevel vorticity tendency (Fig. 7a) is dominated by the horizontal PVA term between 500 and 700 hPa at 1200 UTC on 18 September (Fig. 7b), the contribution of which is slightly negated by the stretching and tilting terms (i.e., Figs. 7d and 7e). (ii) The low-level ζ_a tendency maximum at 925 hPa (Fig. 7a) is predominantly contributed by the stretching term (Fig. 7d), which arises from the compaction of the vorticity field by the low-level convergence (see Figs. 6a and 6c). (iii) The upper-level (300 hPa) ζ_a tendency maximum after 20 September can be mostly explained by the contribution from both horizontal and vertical vorticity advects (Figs. 7b,c). (iv) The tilting term plays no significant role in vorticity production except at the upper levels, where it is offset by the negative contribution from the vertical advection and stretching terms. One should note that the vertical vorticity ad-

vection in Fig. 7c around 400 hPa at 1200 UTC on 20 September results from the transport of positive vorticity from low to midlevels by upward motion within the disturbance, which implies that the source of the disturbance vorticity is at low to midlevels (the primary source being the wave vorticity enhanced by the cyclonic shear to the south of the midlevel jet at 700 hPa mentioned earlier). *Thus these vorticity budget calculations suggest that the low-level convergence within the monsoon confluence zone acted upon a preexisting low-level vortex to increase the low-level vorticity of the disturbance; whereas the midlevel vorticity of the disturbance is enhanced by the PVA on the cyclonic shear side of the jet but ahead of the trough axis (as shown previously), which is then transported upward by the ascending motion within the disturbance.* Therefore, it appears that the merger of the low-level vorticity center (associated with the monsoon shear line) and the midlevel vorticity center (associated with a wave trough to the south of MLEJ maintained by the Saharan dust

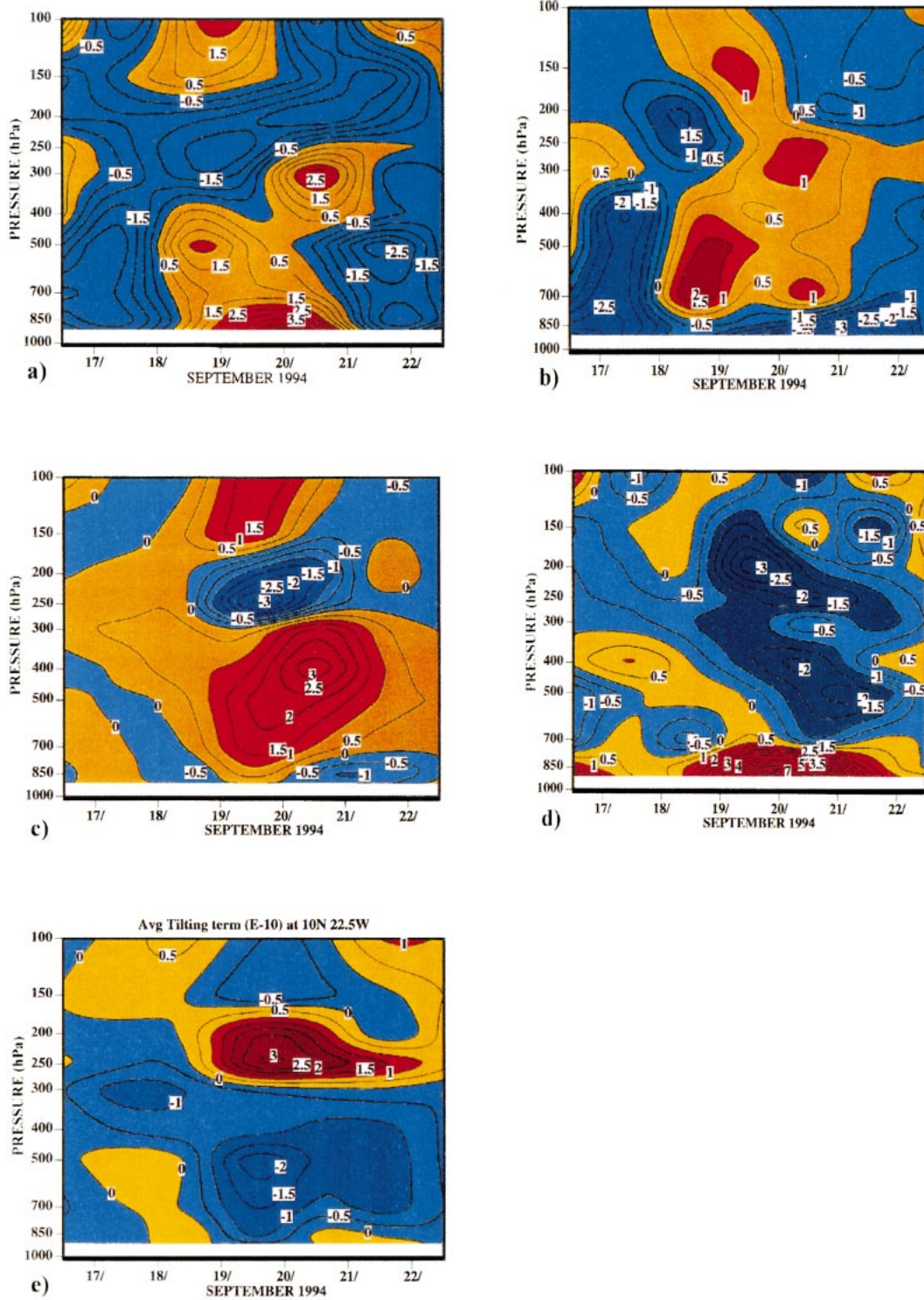


FIG. 7. Same as in Fig. 6 except for the vorticity budget terms: (a) absolute vorticity time tendency [contours (positive, yellow to red; negative, blue) at $0.5 \times 10^{-10} \text{ s}^{-2}$], (b) horizontal absolute vorticity advection [contours (positive, red; negative, blue) at $0.5 \times 10^{-10} \text{ s}^{-2}$], (c) vertical absolute vorticity advection [contours (positive, red; negative, blue) at $0.5 \times 10^{-10} \text{ s}^{-2}$], (d) stretching term [contours (positive, red; negative, blue) at $0.5 \times 10^{-10} \text{ s}^{-2}$], and (e) tilting term [contours (positive, red; negative, blue) at $0.5 \times 10^{-10} \text{ s}^{-2}$].

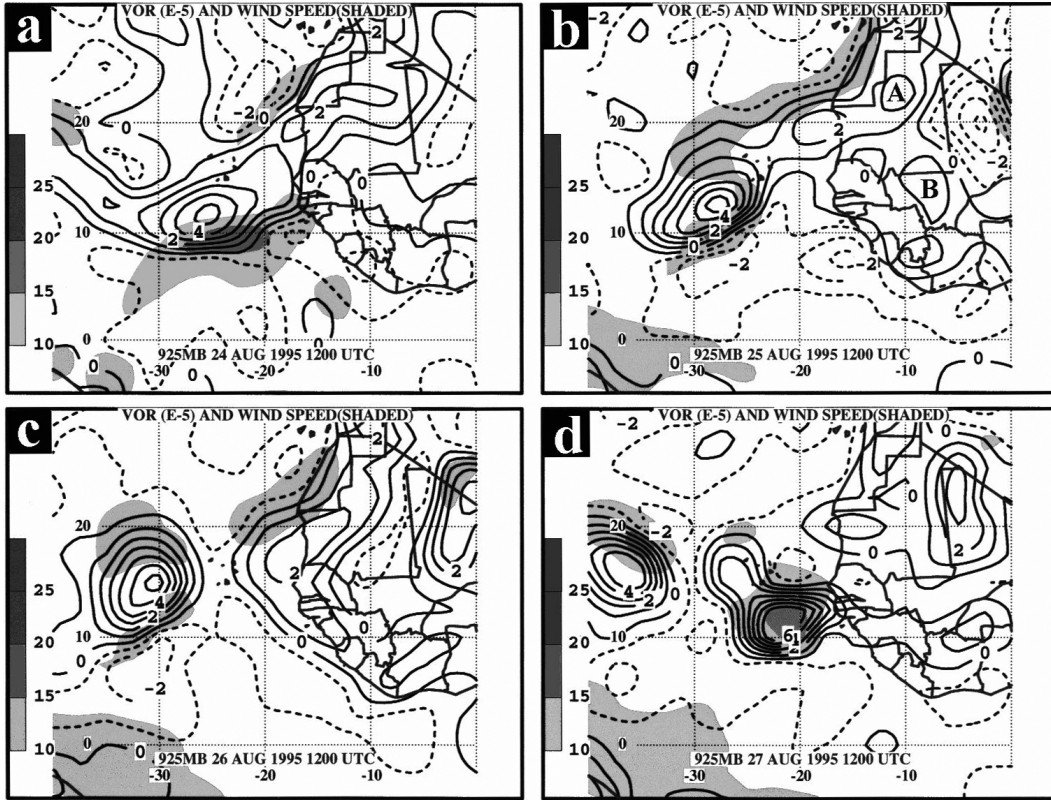


FIG. 8. Same as in Fig. 2 except for Hurricane Luis valid for 24–27 Aug 1995. Letters A and B, respectively, denote the northern and southern vortices referred to in the text.

outbreak) in conjunction with favorable upper-level divergence initiated the genesis process of Ernesto at 1200 UTC 19 September, at least 2 days prior to its declaration of a tropical depression by the Tropical Prediction Center (TPC). This conclusion does not preclude the role of mesoscale vortex merges such as those described by Simpson et al. (1997) in the genesis of Ernesto, which might have aided further development of Ernesto through mesoscale interactions (i.e., stage 2 of the genesis process defined earlier). However, one can argue that large-scale features such as the African wave and Saharan dust outbreak in conjunction with the 700-hPa middle-level jet controlled the large-scale dynamics (i.e., stage 1 of the genesis process). One should also note that the contribution of the MLEJ, forced by the SAL (via positive horizontal temperature gradient at 850 hPa), in enhancing the vorticity of the disturbance through cyclonic shear to the south of the jet, including the role of the resulting positive vorticity advection in the disturbance growth to the south of the SAL, is consistent with the baroclinic mechanism (i.e., items 1–3 of the baroclinic mechanism presented in section 1). However, the merger of low-level vortex with the mid-level vortex in the formation of a deep vortex is a new finding that is different than that proposed in the baroclinic mechanism (i.e., item 4 of the baroclinic mech-

anism involving CISK; see modifications to the baroclinic mechanism in section 5).

b. Hurricane Luis (1995)

Another case that occurred during the normal Sahel rainfall years is Hurricane Luis. Luis originated from an African wave and circulation of low clouds on 26 August 1995 between the West African coastline and the Cape Verde Islands and attained tropical depression status 1 day later near Cape Verde Islands ($\sim 11^{\circ}\text{N}$, 22.7°W) with a central pressure of 1010 hPa. It further strengthened to a tropical storm on 29 August and became a hurricane 1 day later as it subsequently intensified to a category 4 [Saffir–Simpson scale; Simpson (1974)] hurricane by 3 September. Hurricane Luis, which formed over the eastern Atlantic, was the last in a succession of three tropical cyclone formations (Humberto, Karen, and Luis). Both Karen and Luis formed from consecutive wave troughs; however, Karen formed farther west than Luis.

The evolution of Luis's precursor can be seen in the 925-hPa relative vorticity field during the 24–27 August 1995 period (Figs. 8a–d) as its initial vortex at 1200 UTC 25 August (location B in Fig. 8b) develops into a maximum relative vorticity center ($>6 \times 10^{-5} \text{ s}^{-1}$) at

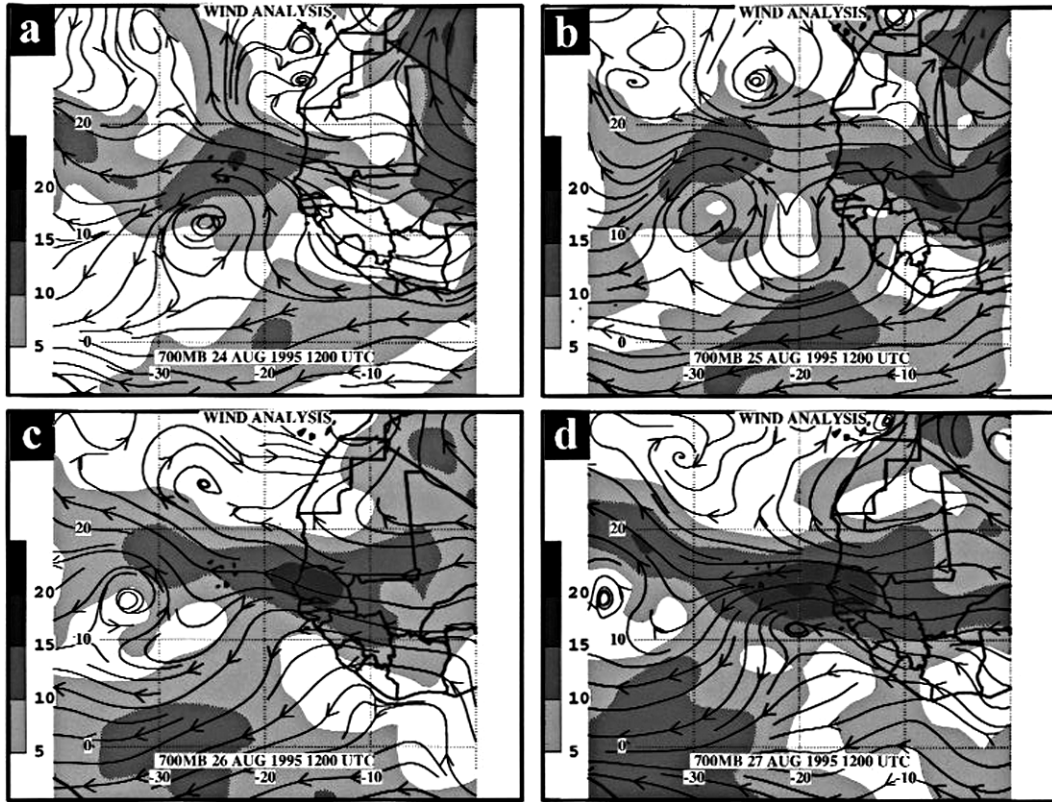


FIG. 9. Same as in Fig. 3 except for the Luis case for 24–27 Aug 1995.

about 11°N , 22°W by 1200 UTC 27 August (Fig. 8d). Similar to Ernesto, this maximum relative vorticity formed along a confluence line that is oriented along the southwest coastline of West Africa (not shown). However, the significant difference between the Ernesto and Luis environmental fields is that the Luis low-level circulation (e.g., ζ of Luis is $>6 \times 10^{-5} \text{ s}^{-1}$; Fig. 8d) is much stronger than that of Ernesto ($>2 \times 10^{-5} \text{ s}^{-1}$; Fig. 2d) (discussed further in section 5).

Although it appears that Luis formed within the monsoon confluence line similar to Ernesto, a close inspection of the 925-hPa ζ field (Figs. 8b–d) suggests that the low-level vortex center of Luis has origins not only over West Africa within the equatorial rainbelt (easterly wave disturbance marked by letter B in Fig. 8b) but also in the monsoon trough over northwest Africa in association with a surface heat low amplified by a low-level jet⁵ [i.e., the vortex center denoted by letter A to the south of the wind maximum ($>10 \text{ m s}^{-1}$) off the coast of northwest Africa in Fig. 8b]. Note that the vorticity associated with the monsoon trough to the north is stronger than the one to the south, perhaps due

to the cyclonic shear associated with the low-level jet. The existence of two low-level vorticity source regions for African wave disturbances is consistent with previous studies (Carlson 1969b; Burpee 1975; Reed et al. 1977). In accordance with these studies, these two low-level vortices from West Africa (see the two separate cyclonic circulations in Fig. 8b over West Africa) merge along the West African coastline (Fig. 8c) and subsequently become the stronger circulation of Luis's precursor (Fig. 8d).

The midlevel vortex evolution of Luis can be seen in the 700-hPa wind field (Figs. 9a–d), which clearly depicts not only the westward propagation of the trailing wave trough (axis oriented in the northwest–southeast direction) from about 8°W at 1200 UTC on 25 August to $\sim 20^{\circ}\text{W}$ on 27 August but also its growth in amplitude to the south of the MLEJ, particularly during 25–27 August. Most importantly, these charts portray the migration of the MLEJ in conjunction with the trailing wave trough as the strength of the jet increases from $>15 \text{ m s}^{-1}$ (at 1200 UTC 25 August; Fig. 9b) to a maximum of $>20 \text{ m s}^{-1}$ (at 1200 UTC 27 August; Fig. 9d). Note that this jet is stronger than that in the Ernesto case and is located directly to the north of the genesis region of Luis by 1200 UTC 27 August. As in Ernesto, this jet consists of both horizontal and vertical wind shears and is collocated with the maximum meridional

⁵ This low-level jet appears to be a manifestation of a strong pressure gradient induced by sensible heating over the Sahara and modulated by the cyclical passage of wave disturbances (Karyampudi 1986).

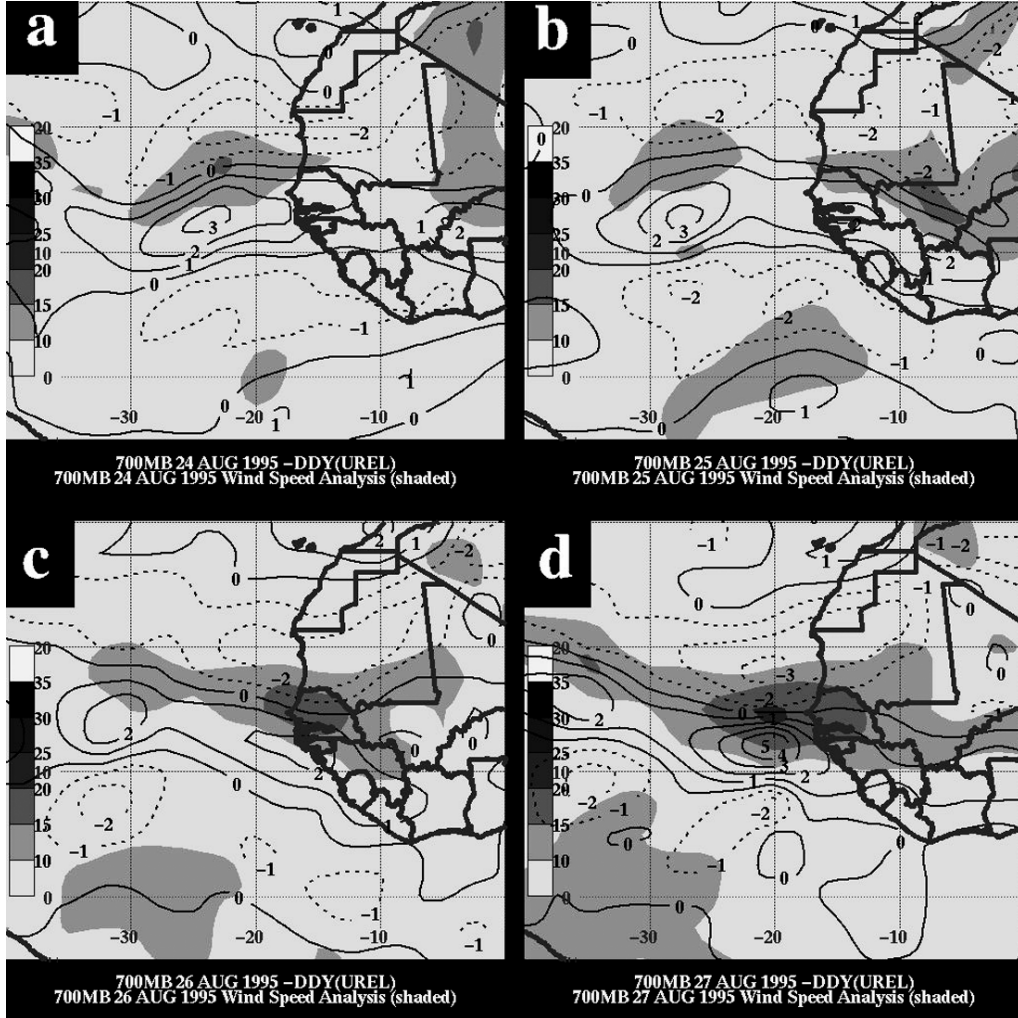


FIG. 10. Same as in Fig. 5 except for the Luis case for 24–27 Aug 1995.

temperature gradient at the 850-hPa level (not shown). Furthermore, this jet is located, as in Ernesto, to the south of an SAL anticyclonic eddy (as described by Karyampudi and Carlson 1988), whose center can be seen tracking westward along 24°–26°N between 25 and 27 August [Figs. 9b–d; note that Karen (i.e., the leading wave disturbance) appeared to have formed at the leading edge of the Saharan anticyclonic eddy as can be seen in Fig. 9c around 30°W].

A broad belt of cyclonic shear vorticity exists to the south of MLEJ, similar to Ernesto, as can be seen in Fig. 10. A cyclonic shear vorticity center of $>2 \times 10^{-5} \text{ s}^{-1}$, which coincides with the disturbance trough axis at $\sim 10^\circ\text{N}, 8^\circ\text{W}$ at 1200 UTC 25 August (Fig. 10b), migrates westward in concert with the wind maximum associated with the MLEJ and intensifies to $5 \times 10^{-5} \text{ s}^{-1}$ at about $12^\circ\text{N}, 20^\circ\text{W}$ by 1200 UTC 27 August (Fig. 10d). [Note that this cyclonic shear vorticity maximum constitutes most of the disturbance vorticity (not shown), as in the case of Ernesto.] The juxtaposition of

this midlevel vorticity maximum with the low-level vorticity maximum at the time of the genesis (i.e., at 1200 UTC 27 August) defines the formation of Luis's precursor.

As in Ernesto, the MLEJ is associated with cross-(isotach/vorticity) contour flow ahead of the wave trough but to the south of the wind speed maximum, significantly between 1200 UTC 26 August and 1200 UTC 27 August (cf. Figs. 9c and 9d, respectively, with Figs. 10c, and 10d). At the time of genesis (i.e., at 1200 UTC 27 August), the cross-contour flow defines wave amplification as it coincides with the low-level cyclonic center located at $11^\circ\text{N}, 22^\circ\text{W}$ (see Figs. 8d and 9d). This cross-vorticity-contour flow across the 700-hPa wave trough axis prior to and during genesis suggests a likely role for the positive vorticity advection to the south and west of the MLEJ (i.e., in the left exist quadrant of the jet) in the genesis of Luis (discussed further later). Note that the plausible role of positive vorticity advection in the wave amplification is similar to the nonlinear vor-

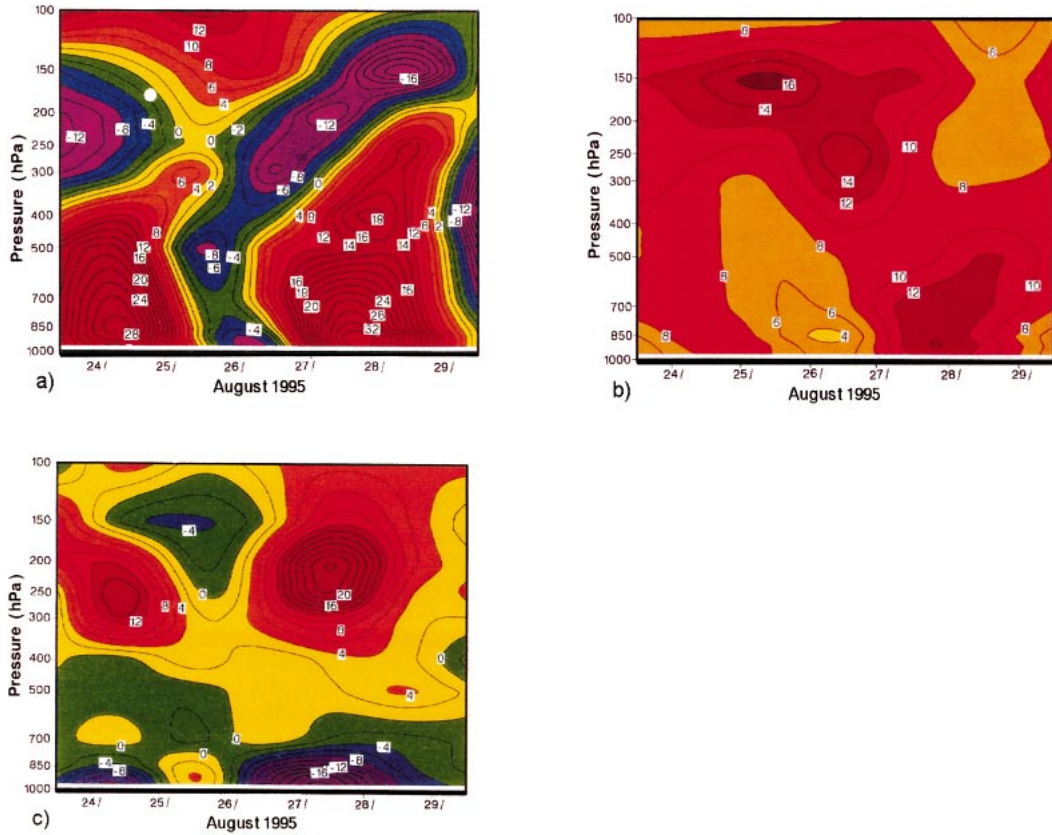


FIG. 11. Same as in Fig. 6 except for the Luis case for 23–29 Aug 1995: (a) ζ [contour (positive is red; negative is green and purple) at $2 \times 10^{-6} \text{ s}^{-1}$], (b) wind speed [contour lines: 2 m s^{-1}], and (c) divergence (div) [contour (positive, red; negative, green and purple) at $2 \times 10^{-6} \text{ s}^{-1}$].

ticity advection emphasized by Shapiro (1977) in the dynamic transformation of a preexisting wavelike disturbance to an intensifying depression.

The vertical structure of the disturbance can be viewed in the time sections of area-averaged ζ , wind speed, and divergence fields (Fig. 11) taken between 23 and 29 August at 12.5°N , 22.5°W (i.e., refer to Fig. 8d for the Luis genesis location). These time sections reveal the following features. (i) The maximum vorticity of Luis (as well as the leading wave disturbance, TS Karen), as in Ernesto, is at low levels (i.e., $>32 \times 10^{-6} \text{ s}^{-1}$ at 925 hPa close to 0000 UTC 28 August; Fig. 11a). (ii) The maximum low- to midlevel relative vorticity axis (Fig. 11a) is collocated with the axis of the wind maximum (defined by the 12 m s^{-1} contour), which extends from the surface to 500 hPa (Fig. 11b). (iii) An upper-tropospheric easterly jet ($>16 \text{ m s}^{-1}$) exists at the 150-hPa level, at least 2 days prior to the passage of the vortex center (i.e., at 1200 UTC 25 August; Fig. 11b). (iv) Upper-level divergence ($\sim 200 \text{ hPa}$) and low-level convergence (\sim surface) correspond well (Fig. 11c), respectively, with the upper-level anticyclonic and low-level cyclonic vorticity (Fig. 11a) fields for both Luis and Karen. Note that, in contrast to Ernesto, there is no persistent large-scale upper-level anticyclonic cir-

culation over the genesis region of Luis as revealed by the 200-hPa streamline and divergence fields (not shown). Instead only northeasterly flow existed over the Luis genesis region 24 h prior to its formation. The transient anticyclonic circulation center, however, existed farther to the west and poleward of Karen's low-level disturbance center (i.e., farther northwest of Luis's low-level disturbance center), which suggests that the upper-level divergence and anticyclonic vorticity (seen in Figs. 11a and 11c) are associated with the disturbance itself rather than with large-scale anticyclonic circulation.

To understand the processes contributing to the growth of the Luis vortex, vorticity budget time sections are shown in Fig. 12. The absolute vorticity time tendency (Fig. 12a) clearly shows that the maximum change to the cyclonic vorticity occurs near the low levels. Most of it appears to be contributed by the stretching term (Fig. 12d) as a result of low-level convergence (refer to Fig. 11c) compacting the disturbance positive vorticity (Fig. 11a) as in the case of Ernesto. However, the lower- to upper-level positive tendency is not only aided by the PVA (Fig. 12b) but also by the vertical advection term as a result of the vertical transport of low-level vorticity by upward motion within the

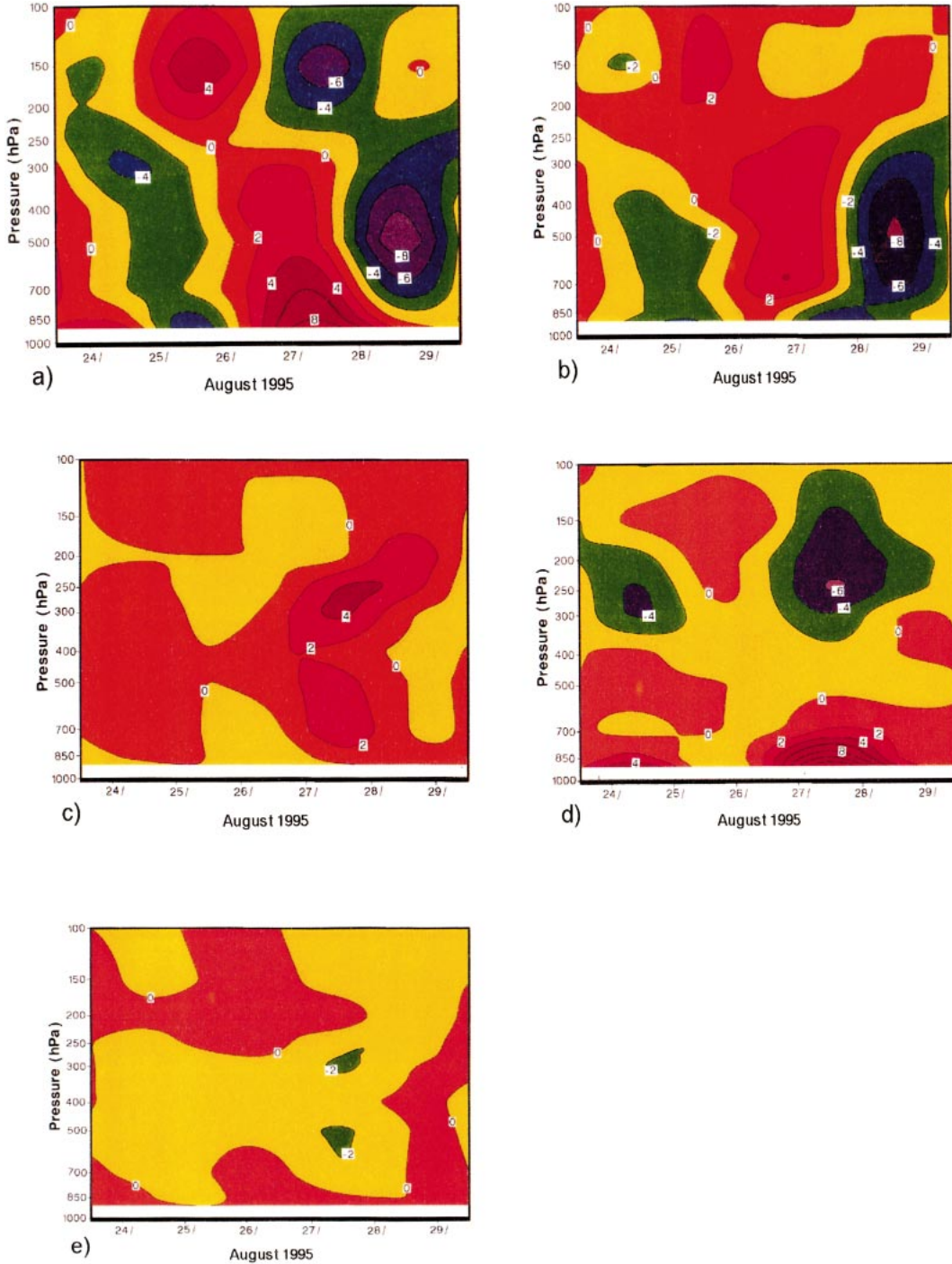


FIG. 12. Same as in Fig. 7 except for the Luis case for 23–29 Aug 1995: (a) absolute vorticity time tendency [contours (positive, red; negative, green and purple) at $2 \times 10^{-10} \text{ s}^{-2}$], (b) horizontal absolute vorticity advection [contour (positive, red; negative, green and purple) at $2 \times 10^{-10} \text{ s}^{-2}$], (c) vertical absolute vorticity advection [contour (positive, red; negative, yellow) at $2 \times 10^{-10} \text{ s}^{-2}$], (d) stretching term [contour (positive, red; negative, green and purple) at $2 \times 10^{-10} \text{ s}^{-2}$], and (e) tilting term [contours (positive, red; negative, green) at $2 \times 10^{-10} \text{ s}^{-2}$].

disturbance (Fig. 12c), similar to that in Ernesto. The PVA arises from the cyclonic shear vorticity advection on the forward edge of the disturbance (note that the small maximum $>3 \times 10^{-10} \text{ s}^{-2}$ located at 700 hPa at about 1200 UTC 27 August can be explained by the PVA on the left-forward quadrant of the MLEJ as inferred previously from Figs. 9d and 10d). The positive contribution by the vertical advection term at upper levels (i.e., ~ 300 hPa at 1200 UTC 27 August; Fig. 12c), however, is nullified by the negative contribution from the stretching term (Fig. 12d). As in Ernesto, the contribution from the tilting term appears to be negligible (Fig. 12e). It should be mentioned that the dominant contributions by vortex stretching in the lower levels and horizontal vorticity advection in the lower to upper troposphere are consistent with other studies such as that of Kurihara and Tuleya (1981), who showed in their numerical study of tropical storm genesis that these respective processes are a major component of the vorticity tendency of a developing vortex (at the depression stage).

From the above analyses, one can infer that Luis's midlevel cyclonic vorticity is enhanced by the cyclonic shear associated with the MLEJ that appears to be maintained by the maximum temperature gradient provided by the SAL anticyclonic eddy, as in the case of Ernesto. *The growth of the midlevel vorticity of Luis appears to be dominated mostly by cyclonic shear vorticity advection arising from cross- (vorticity) contour flow across (i.e., on the south and west side of) the MLEJ but just ahead of the trough axis; whereas the development of the low-level vorticity is mostly provided by the low-level convergence acting upon the low-level disturbance vorticity.* One should note that the processes involved in the growth of the midlevel vortex through the interaction of the SAL with the African wave disturbance are consistent with the baroclinic mechanism as in the case of Ernesto. On the other hand, the divergence and vorticity patterns associated with Luis (convergence below and divergence above) appear to reflect an outflow region from deep convection as no clear evidence is found of the prior existence of persistent upper-level divergence. Therefore, one can say that Luis is self-maintained with little external upper-level forcing needed to initiate genesis other than low- to midlevel forcing arising from the baroclinic mechanism (this aspect will be discussed further in section 5). Nevertheless, the role of mesoscale convective vortices in the genesis of Luis cannot be discounted.

c. Hurricane Andrew (1992)

The precursor of Hurricane Andrew is an easterly wave that emerged from the west coast of Africa on 14 August 1992 embedded within a deep easterly current on the south side of an upper-level high pressure system. It passed the Cape Verde Islands the following day and attained tropical depression status a day later by 1800

UTC 16 August when its central pressure reached 1010 hPa at 10.8°N , 35.5°W . Andrew subsequently became a hurricane over the western Atlantic and caused billions of dollars damage and 15 fatalities within the United States (most of it over the southern Florida peninsula) as it attained category 4 hurricane status with 922-hPa central pressure at landfall over the United States (Mayfield et al. 1994). Andrew was the only hurricane that formed over the eastern Atlantic in 1992.

As in Ernesto and Luis, the genesis of Andrew can be identified from the 925-hPa relative vorticity field between 12 and 15 August 1992 (Figs. 13a–d). These figures clearly show the strengthening of low-level cyclonic vorticity of an African wave from its initial cyclonic vorticity of $>1 \times 10^{-5} \text{ s}^{-1}$ centered around 13°N , 7°W [see the plus sign (+) in Fig. 13a] to $>2 \times 10^{-5} \text{ s}^{-1}$ at about 10°N , 20°W by 1200 UTC 15 August [Fig. 13d; at this time the 925-hPa streamline field clearly exhibited a cyclonic circulation signature (not shown)]. The cyclonic shear of a wind surge (i.e., the wind maximum $>10 \text{ m s}^{-1}$ located to the southeast of the vorticity center) in Fig. 13d, which is associated with the southwesterly monsoon flow (not shown), appears to have contributed to the increase of the low-level cyclonic vorticity of Andrew by 1200 UTC 15 August.

The 700-hPa wind field in Fig. 14 clearly shows the evolution of Andrew from a weak African wave along 7°W at 1200 UTC 12 August (Fig. 14a) to a cyclonic circulation at about 7°N , 19°W by 1200 UTC 15 August (see Fig. 14d). These charts also depict the strengthening of a weak MLEJ ($>10 \text{ m s}^{-1}$), to the north of the trough axis (i.e., to the north of 10°N , 7°W in Fig. 14a), into a broad wind maximum ($>15 \text{ m s}^{-1}$) to the northwest of Andrew's cyclonic circulation by 1200 UTC 15 August. Although an MLEJ wind maximum is present to the north of Andrew's precursor as in the Ernesto and Luis cases, a close comparison of the wind fields between Andrew (Fig. 14) and Ernesto (Fig. 3)/Luis (Fig. 9) reveals the following differences. (i) The amplitudes of the African waves in Andrew appear to be weaker (due to less perturbed easterly flow than the more perturbed African waves of Ernesto and Luis). (ii) The middle-level easterly jet (as can be identified by the isotach contour $>10 \text{ m s}^{-1}$) appears to be broader and possesses multiple wind maxima to the north of the Andrew's precursor prior to its formation (see multiple wind maxima in Figs. 14b and 14c), in contrast to a narrow wind maximum present in the Ernesto and Luis cases (refer to Figs. 3 and 9, respectively). (iii) The broad-scale easterly flow in Andrew does not clearly exhibit the characteristic anticyclonic SAL eddy to the north of the jet that was present in both the Ernesto and Luis cases to the north of 20°N , as was mentioned. In fact, the less perturbed easterly flow (which extended well into the upper troposphere) appeared to favor a continuous SAL that is wider ($10^\circ\text{--}30^\circ\text{N}$ over much of the western Africa and eastern Atlantic region) and deeper (extended up to 500 hPa) as noted from cross

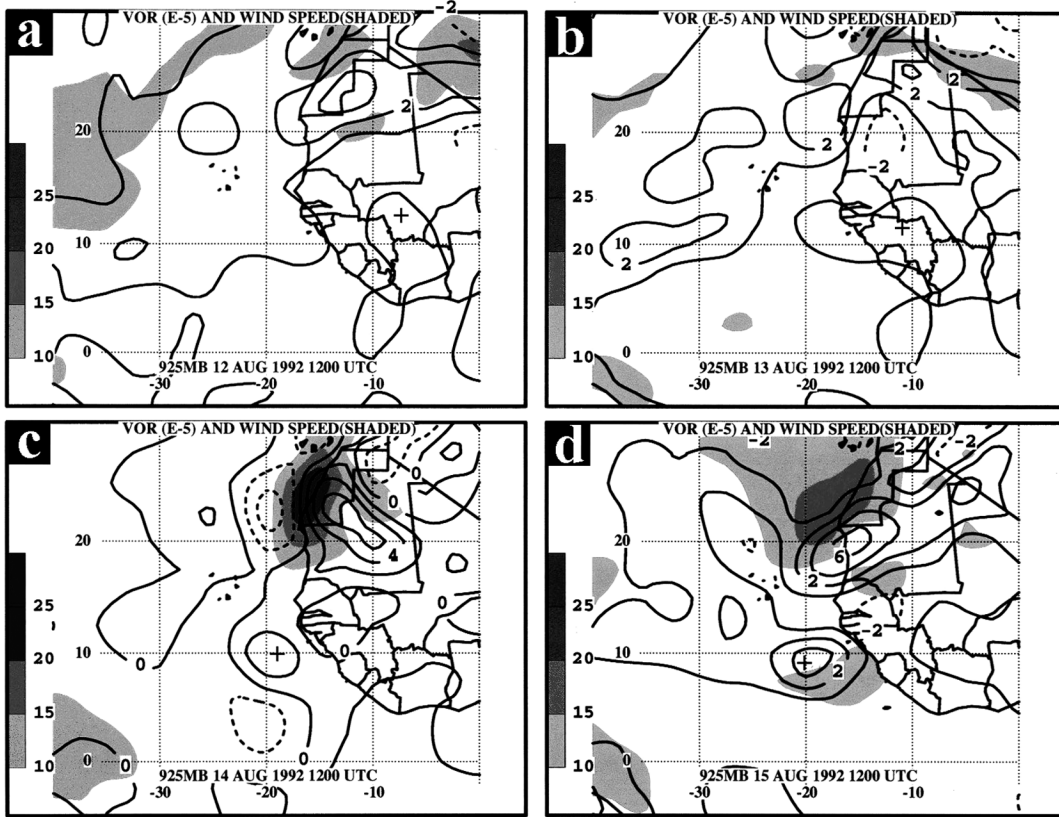


FIG. 13. Same as in Fig. 2 except for Hurricane Andrew valid for 12–15 Aug 1992. The plus sign (+) denotes the low-level cyclonic circulation center as noted from the 925-hPa streamline analysis.

sections and soundings taken to the north of Andrew's precursor (i.e., north of 10°N ; not shown).

Most importantly, the less perturbed easterly flow with weaker cyclonic shear in Andrew appears to result in a weaker cyclonic shear vorticity as can be seen in Fig. 15; compare the cyclonic shear vorticity maximum of $>2 \times 10^{-5} \text{ s}^{-1}$ in Fig. 15d with the cyclonic shear vorticity maximum of $>3 \times 10^{-5} \text{ s}^{-1}$ for Ernesto (Fig. 5d) and $>6 \times 10^{-5} \text{ s}^{-1}$ for Luis (Fig. 10d). Furthermore, the weaker cross- (vorticity) contour flow arising from the less perturbed easterly flow across the weaker cyclonic shear vorticity to the south of the jet in Andrew appears to contribute to weaker positive vorticity advection, as can be deduced by comparing Figs. 14 and 15 for Andrew with the corresponding figures for Ernesto (Figs. 3 and 5) and for Luis (Figs. 9 and 10). Nevertheless, the broader MLEJ wind maximum (to the north of Andrew at 1200 UTC 15 August) overlaps the 850-hPa meridional temperature gradient maximum (not shown) as in the Ernesto and Luis cases.

Vertical time sections of area-averaged vorticity, wind speed, and divergence fields taken at 10°N , 22.5°W (i.e., Andrew genesis location) between 12 and 18 August (Fig. 16) reveal that the relative vorticity maximum of Andrew's precursor is at low levels as in the case of Luis ($\zeta > 20 \times 10^{-6} \text{ s}^{-1}$ at 850 hPa; Fig. 16a), even

though the cyclonic vorticity core ($>16 \times 10^{-6} \text{ s}^{-1}$) spreads to the level of MLEJ (700 hPa) as positive relative vorticity associated with the vortex itself extends to 200 hPa. The mean wind speed (Fig. 16b) associated with the MLEJ at 700 hPa appears as a downward extension of the upper-tropospheric easterly jet in contrast to separate low- to midlevel (MLEJ) wind maxima in the Ernesto and Luis cases (cf. Fig. 16b with Figs. 6b and 11b). The upper-level jet coincides with the upper-level divergence, which appears to persist at least 2 days prior to the occurrence of the precursor at that location (Fig. 16c). However, the vortex itself is defined by weak convergence below and weak divergence above as the upper-level anticyclonic vorticity that is typically required for further development is rather weak. The anticyclonic vorticity appears to be rather weak since the disturbance is embedded in a deep easterly current that is dominated by anticyclonic circulation farther to the north as revealed by the 200-hPa streamline and divergence fields (not shown). Thus these fields suggest that the vortex, which has high values of low-level vorticity with weak convergence at low levels and weak divergence aloft without a well-defined upper-level anticyclone over the disturbance center, appears rather unorganized compared to Luis's precursor, which may ex-

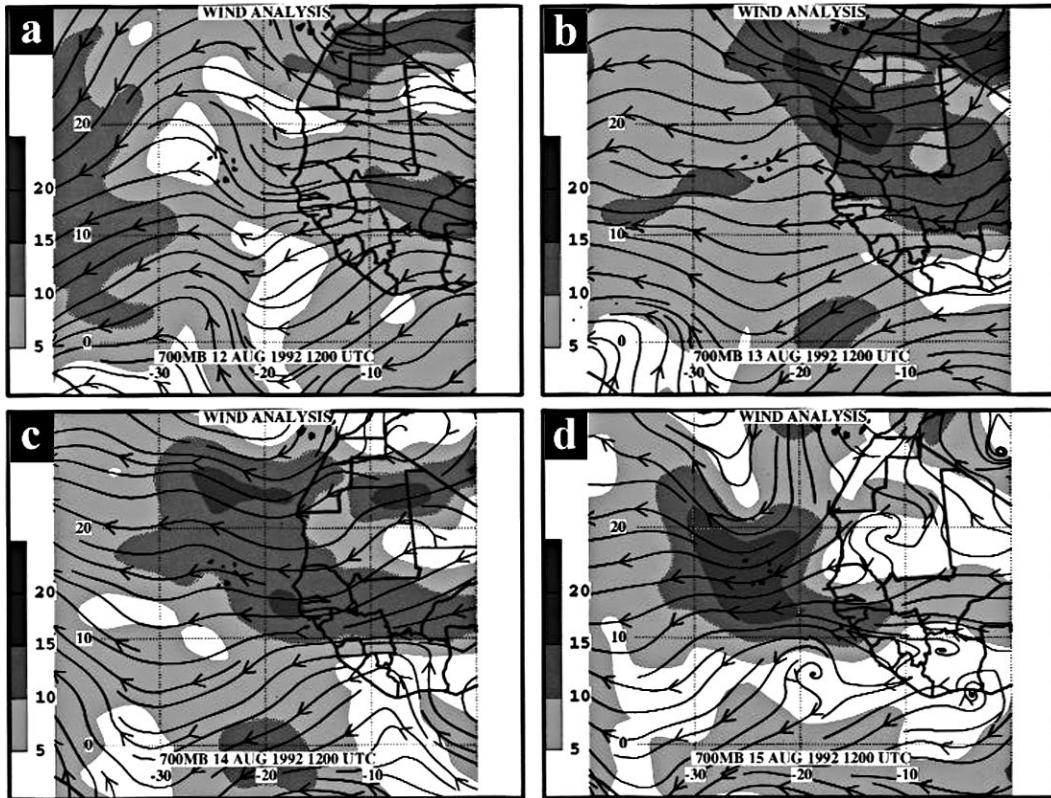


FIG. 14. Same as in Fig. 3 except for the Andrew case for 12–15 Aug 1992.

plain why Andrew remained weak until reaching the Bahamas to become a hurricane.

The vorticity budget time sections at the same location given in Fig. 17 show that the positive tendency (Fig. 17a) ahead of the disturbance can be explained mostly by the horizontal positive vorticity advection (Fig. 17b), particularly in the mid- to upper troposphere. It is interesting to note that the horizontal vorticity advection, though it is positive, does not exhibit a maximum at 700 hPa (i.e., the level of the MLEJ) since no significant downshear flow across the cyclonic shear vorticity exists to the south of the MLEJ at 700 hPa (refer to Figs. 14c,d) as mentioned earlier. Note that the weak PVA at 700 hPa in Andrew contrasts sharply with the maximum PVA at the same level in the Ernesto and Luis cases (cf. Fig. 17b with Figs. 7b and 12b). Instead, the PVA in Andrew exhibits a maximum at upper levels (~ 200 hPa), which is the largest contribution to the total vorticity tendency (see Fig. 17b). Inspection of the streamline and wind speed charts at 200 hPa (not shown) suggests that this maximum PVA appears to result from the extension of easterly wave perturbations to the upper troposphere on the equatorward side of an upper-level anticyclonic circulation center but to the north of an upper-level easterly jet.

At low levels, the contribution to the vorticity tendency is furnished mostly by the stretching term (Fig. 17d) as in the Ernesto and Luis cases. The stretching

term also contributes positively at midlevels but it is smaller in magnitude than at low levels. The vertical advection of horizontal vorticity, on the other hand, contributes positively to the vorticity tendency at mid- to upper levels (see Fig. 17c), which appears to be provided by the vertical transport of low-level vorticity by upward motion within the disturbance, as in the Ernesto and Luis cases. Much of the upper-level positive vertical vorticity advection, however, appears to be neutralized by the negative augmentation by the stretching and tilting terms (Figs. 17d,e); the overall contribution of the latter is negligible, however. *Thus, by comparing these analyses with those from the Ernesto and Luis cases, one can infer the following: The baroclinic mechanism plays an insignificant role in Andrew's case due to weak cyclonic shear vorticity advection by negligible cross-(vorticity) contour flow across a broad mid-tropospheric jet that is embedded within a less perturbed zonal flow compared to the other two cases (the role of SAL is discussed in section 5).*

4. Combined barotropic–baroclinic instability

In the previous sections, evidence was presented that tropical cyclogenesis occurred as a result of the merger of low- and midlevel vortices in at least two (i.e., Ernesto and Luis) out of the three cases examined. It was also shown that the middle-level vortices were enhanced

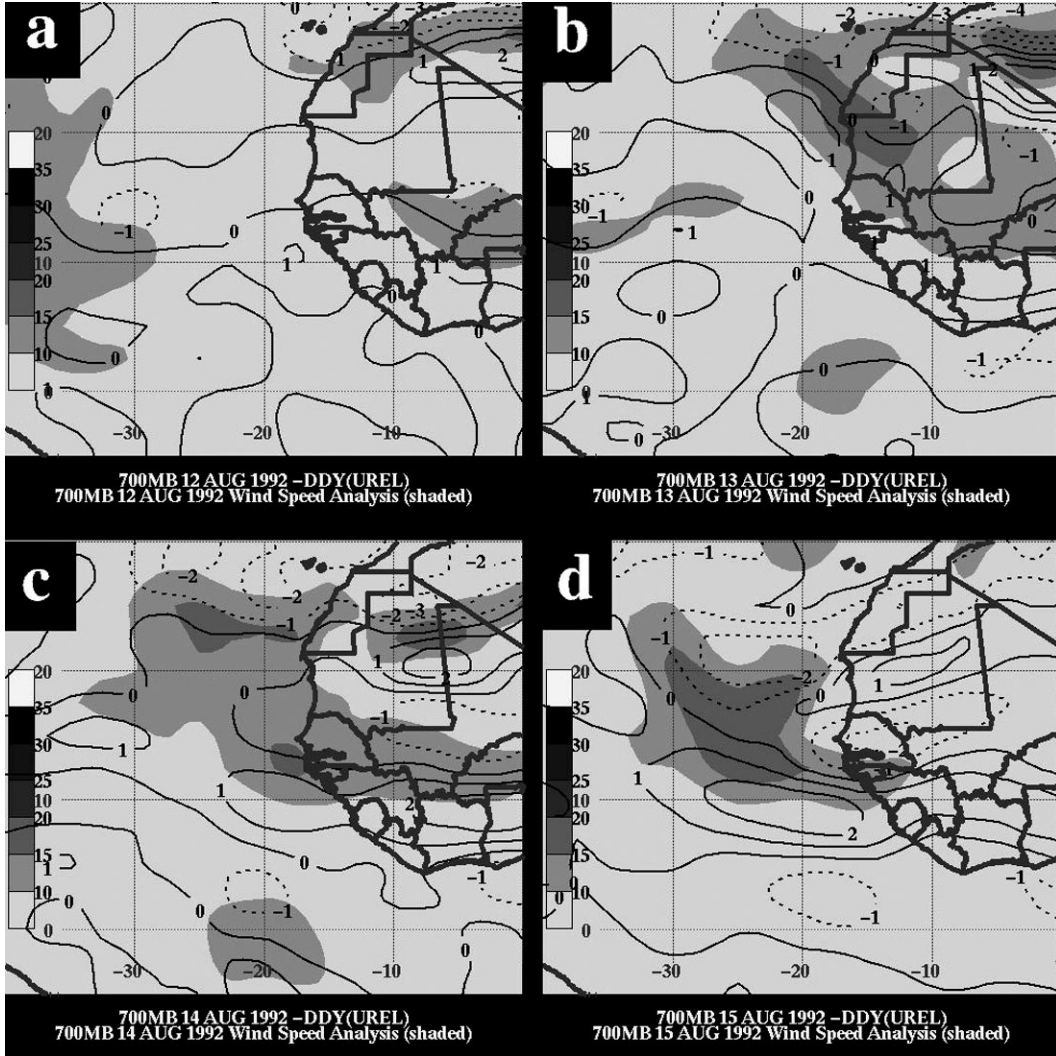


FIG. 15. Same as in Fig. 5 except for the Andrew case for 12–15 Aug 1992.

by the cyclonic shear to the south of the middle-level jet, which was found to be associated with both horizontal and vertical shears in conjunction with a north-south horizontal potential temperature gradient at the 850-hPa level across the base of the SAL.

The presence of vertical and horizontal shears in conjunction with horizontal temperature gradients implies that barotropic and baroclinic instability might be playing a role in the growth of these disturbances. Previously, Burpee (1972) showed that the sign reversal of the meridional potential vorticity gradient on an isentropic surface over North Africa satisfied the Charney and Stern (1962) condition for the combined barotropic and baroclinic instability of the internal jet, which implied that both horizontal and vertical shears associated with the midtropospheric jet are important sources of energy for African wave growth. In order to find out whether the combined barotropic and baroclinic instability is playing a role in the wave growth of any of the

three cases, mean meridional PV gradients were evaluated between the 700- and 850-hPa levels using 7-day-averaged wind and potential temperature fields⁶ as described in section 2. These plots for the all three cases are shown in Fig. 18. It is clear that the mean meridional gradient of potential vorticity reverses sign in all three cases but more significant sign reversals occur over the eastern Atlantic in only two cases—Ernesto and Luis (Figs. 18b,c). These sign reversals extend to the 500–700-hPa layer in all the cases—weaker in the Andrew and Ernesto cases but stronger in the Luis case (not shown).

Recently Throncroft and Blackburn (1999) have shown that the PV sign reversal arises from the destruction of PV due to sensible heating over the Sahara to

⁶ These averages were made for the periods of 12–18 August 1992 for Hurricane Andrew, 16–22 September 1994 for TS Ernesto, and 23–29 August 1995 for Hurricane Luis (centered at the genesis time).

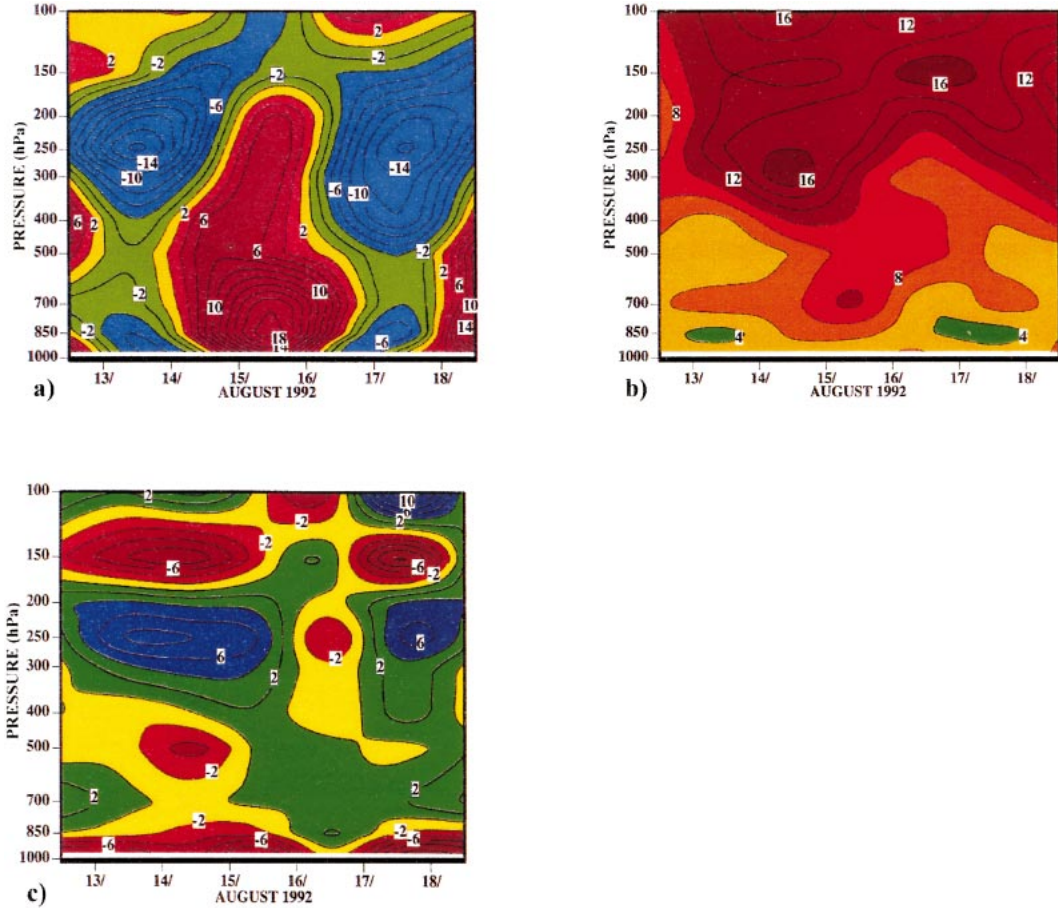


FIG. 16. Same as in Fig. 6 except for the Andrew case for 12–18 Aug 1992: (a) ζ [contour (positive, red; negative, green and purple) at $2 \times 10^{-6} \text{ s}^{-1}$], (b) wind speed [contour lines: 2 m s^{-1}], and (c) divergence (div) [contours (positive, green and purple; negative, red) at $2 \times 10^{-6} \text{ s}^{-1}$].

the north of the jet. Furthermore, Dickinson and Molinari (2000) found that the magnitude of the negative PV anomaly over the Sahara is substantially greater than the positive anomaly to the south. They further suggest that the dry convection (i.e., the convectively driven mixed layer, which we refer to as the SAL) plays a more significant role in the generation of negative sign reversal than does moist convection to the south. On the other hand, Karyampudi and Carlson (1988) have shown that easterly waves advect the SAL downstream of the Sahara as anticyclonic eddies, which result in maximum horizontal potential temperature gradients across the base of the SAL (i.e., at the base of the elevated mixed layer) southern boundary at 850 hPa over the eastern Atlantic. Note that the warm anomaly associated with the SAL base appears in the mean structure of the African waves as well, as can be noted from the composite study of Reed et al. (1977), who attribute the strong temperature contrast at 850 hPa to the warm Saharan air to the north and the cooler air overlying the ocean waters to the south. [Their study further depicts the collocation of the meridional decrease of absolute vor-

ticity with the less stable Saharan air (arising from warm anomaly below and cooler anomaly above) implying the existence of negative PV anomaly to the north of the jet (cf. their Figs. 2b and 2c).]

Cross sections of mean meridional potential temperature gradient fields (taken across the disturbance location of each case between the equator and 30°N), shown in Fig. 19, confirm the existence of maximum positive temperature gradients at 850 hPa in all the three cases. These temperature gradient anomalies exist to the north of the maximum meridional gradient of absolute vorticity ($\delta\zeta_a/\delta y$) but within the negative anomalies of the meridional gradient of absolute vorticity. In particular, the negative meridional gradient of ζ_a anomalies at 700 hPa in Ernesto and Luis (Figs. 19b and 19c) are collocated with the maximum wind speeds associated with the MLEJ (not shown) at about the same level. The positive temperature gradient anomalies, on the other hand, vertically extend to ~ 500 hPa in the case of Andrew (Fig. 19a) and to about 600 hPa in both the Ernesto and Luis cases (Figs. 19b and 19c). The maximum positive temperature gradient anomalies at 850

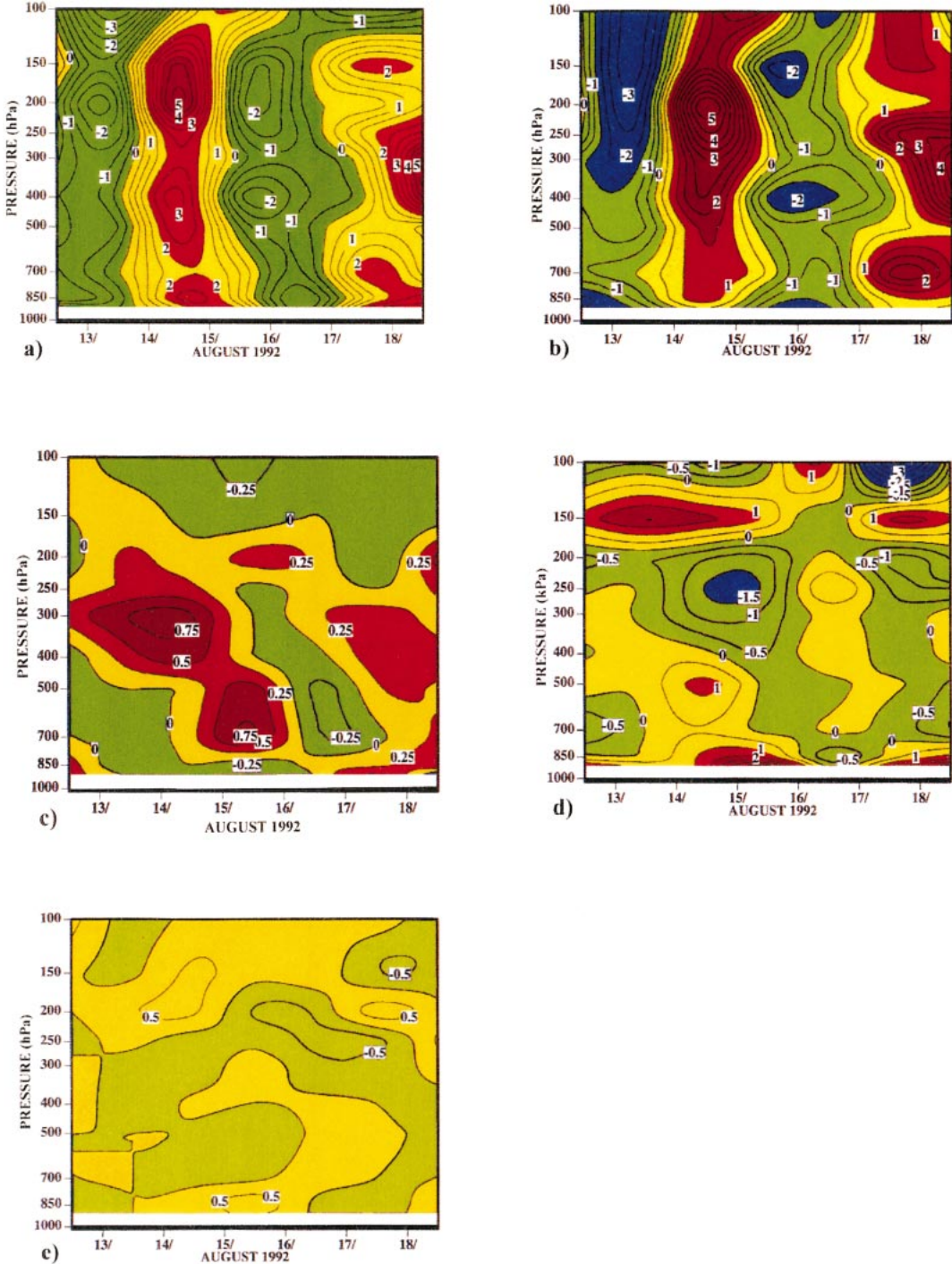


FIG. 17. Same as in Fig. 7 except for the Andrew case for 12–18 Aug 1992: (a) absolute vorticity time tendency [contours (positive, red and yellow; negative, green) at $0.5 \times 10^{-10} \text{ s}^{-2}$], (b) horizontal absolute vorticity advection [contours (positive, red and yellow; negative, light green and blue) at $0.5 \times 10^{-10} \text{ s}^{-2}$], (c) vertical absolute vorticity advection [contours (positive, red and yellow; negative, green) at $0.25 \times 10^{-10} \text{ s}^{-2}$], (d) stretching term [contours (positive, red and yellow; negative, negative green and blue) at $0.5 \times 10^{-10} \text{ s}^{-2}$], and (e) tilting term [contours (positive, yellow; negative, light green) at $0.5 \times 10^{-10} \text{ s}^{-2}$].

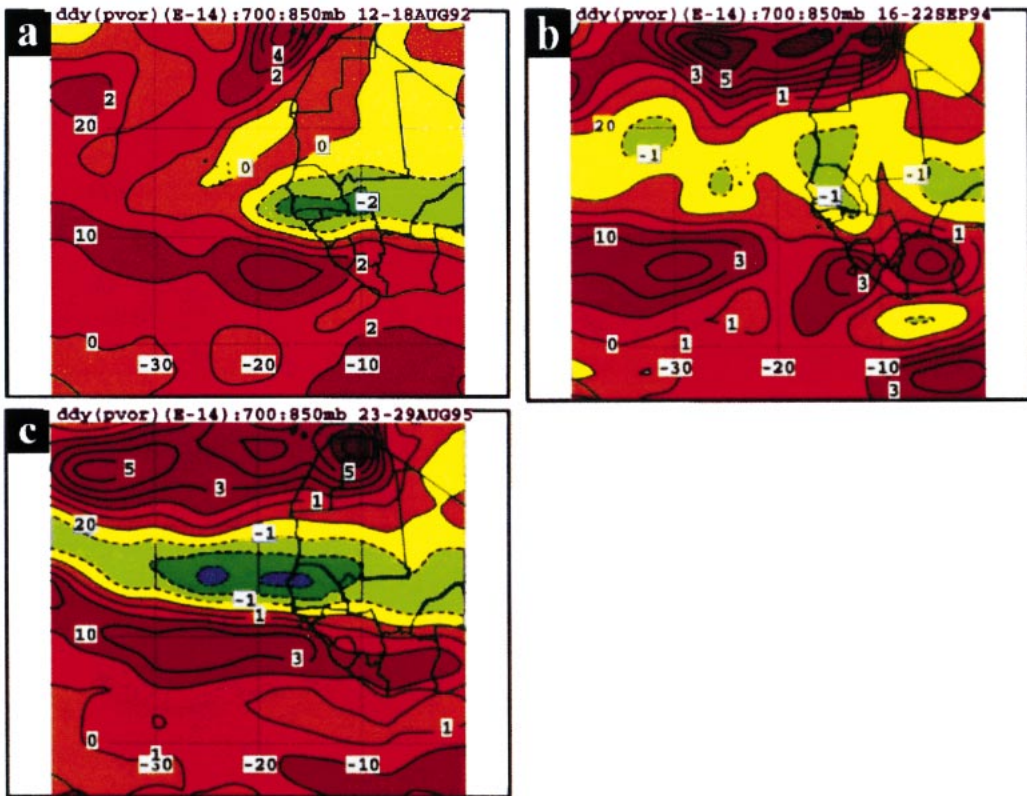


FIG. 18. Mean meridional gradients of potential vorticity within the 850–700-hPa layer for (a) Hurricane Andrew (12–18 Aug 1992), (b) TS Ernesto (16–22 Sep 1994), and (c) Hurricane Luis (23–29 Aug 1995). Contour interval is 1×10^{-14} K hPa $^{-1}$ s $^{-1}$ m $^{-1}$; positive, orange to dark red; negative, yellow to purple. The mean fields were obtained from averages taken over 1-week periods given in the parentheses of each case.

hPa (Fig. 19) define the southern boundary of the SAL; the base of the SAL at 850 hPa can be seen to extend northward from the maximum positive anomalies to the minimum negative anomalies; the widest (from 10°N to at least 30°N) is associated with Andrew and the narrowest is associated with Luis (from 12.5° to 25°N). [Also, note that the occurrence of positive potential temperature gradients in Fig. 19 in conjunction with the negative PV gradient anomalies in Fig. 18 at the same locations is consistent with the occurrence of well-defined SAL anticyclonic eddies to the north of MLEJ over the eastern Atlantic in both the Ernesto and Luis cases as described earlier (refer to section 3).]

The less rapid decrease of potential temperature gradient with height in Andrew than in Ernesto and Luis indicates that the vertical stability of the SAL in Andrew is greater than for those in Ernesto and Luis [cf. the 2×10^{-6} K m $^{-1}$ contour at about the 600-hPa level, above the maximum temperature anomaly, in Andrew (Fig. 19a) to the same contour within the 700–800-hPa layer in Ernesto and Luis (Figs. 19b,c)]. The negative gradient of the ζ_a anomaly in Andrew (Fig. 19a), on the other hand, is located at a lower level (i.e., at the 800-hPa level, just to the south of the maximum temperature gradient anomaly) than in Ernesto and Luis, in which

the gradient is located at 700 hPa (i.e., above the maximum temperature gradient anomaly). Note that the absence of minimum absolute vorticity gradient anomaly in Andrew at 700 hPa appears to be due to an ill-defined MLEJ compared to those in Ernesto and Luis (not shown). The combined effect of a weak meridional gradient of ζ_a at 700 hPa and larger stability (within the 500–850-hPa layer) in Andrew implies that the weak PV gradient anomaly in Andrew over the eastern Atlantic (noted earlier in Fig. 18) is due not only to the weak horizontal wind shear associated with the MLEJ but also due to larger vertical stability associated with the SAL. The larger negative PV anomalies at 700 hPa in Ernesto and Luis, on the other hand, can be explained by the combined influence of less stable SAL (as can be inferred from the rapid decrease of positive temperature gradient anomalies in the vertical in Ernesto and Luis (Figs. 19b,c) and a stronger negative meridional gradient of absolute vorticity anomalies (arising from stronger horizontal wind shears associated with the MLEJ) in the same region. Thus these inferences imply that the stronger negative PV gradient anomalies in Ernesto and Luis are associated with a well-defined (i.e., less stable) SAL, which appears to contribute to the PV sign reversals over the eastern Atlantic in the Ernesto

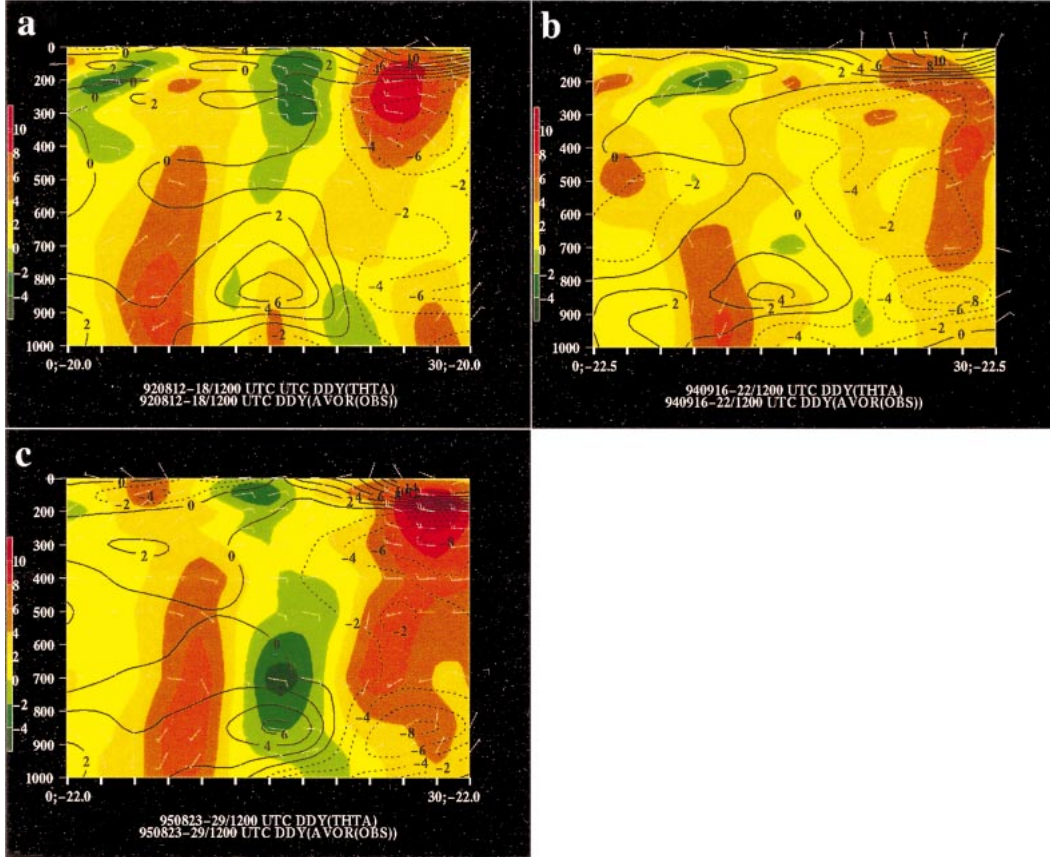


FIG. 19. Mean meridional gradients of potential temperature [contours (negative dashed) at $2 \times 10^{-6} \text{ K m}^{-1}$] and absolute vorticity [contours (positive, yellow, dark yellow, orange, brown, and dark red; negative, light green to dark green) at $2 \times 10^{-11} \text{ s}^{-1} \text{ m}^{-1}$] between the equator and 30°N over the eastern Atlantic for (a) Hurricane Andrew (12–18 Aug 1992), (b) TS Ernesto (16–22 Sep 1994), and (c) Hurricane Luis (23–29 Aug 1995). (Note that each tick mark along the abscissa is equal to 2.5° lat. The ordinate represents pressure in hPa.)

and Luis cases. These PV sign reversals, which satisfy a necessary condition for instability of the mean flow for both the Ernesto and Luis cases, further suggest that the SAL played a significant role in the growth of these two disturbances by contributing to the generation of a negative PV anomaly to the north of the jet. It is interesting to note that the occurrence of the combined barotropic and baroclinic instability in the Ernesto and Luis cases is consistent with the validity of the baroclinic mechanism for the same two cases discussed previously, implying that baroclinic processes are playing an important role in the growth of these wave disturbances.

5. Summary and discussion

Three individual cases, which occurred during the 1992, 1994, and 1995 hurricane seasons [i.e., Hurricane Andrew (1992), TS Ernesto (1994), and Hurricane Luis (1995)], have been diagnostically analyzed using ECMWF gridded data in order to study the genesis mechanisms of tropical cyclones over the eastern At-

lantic. These cases were selected to contrast the differences in the influences of the SAL (i.e., the Saharan dust layer) on tropical cyclogenesis during dry (i.e., 1992) and normal (1994 and 1995) Sahel rainfall years since it is well known that Sahel drought conditions increase the intensity and frequency of Saharan dust (i.e., SAL) outbreaks (Prospero and Nees 1986; Swap et al. 1996). Heavy dust outbreaks, in turn, are perceived to adversely impact the African wave development through suppression of convection over the equatorial regions (e.g., Randall et al. 1984; Karyampudi and Carlson 1988). Analyses of wind fields and other important variables including vorticity budgets (spatially averaged at the genesis location) were presented to understand the genesis processes of all the three cases. In addition, weekly averages of winds and potential temperature fields were made to evaluate the sign reversal of the meridional gradient of potential vorticity necessary for the instability of the zonal flow.

To synthesize the results of all three cases presented in the previous sections, a summary of all the important features derived from synoptic, vorticity budget, and PV

TABLE 1. Summary of genesis features of the Andrew, Ernesto, and Luis cases taken at or near the disturbance center at the time of genesis (second column; time of depression stage in parentheses). The fifth and sixth columns represent meridional component of relative vorticity (cyclonic shear vorticity in parentheses) values at the 925- and 700-hPa levels, respectively. The depth (top numbers in mb) and width (latitude belt) of the SAL are given in column 5 of the bottom panel. The genesis potential, given in the last column, is an area average over a 5° lat \times 5° long box centered on the disturbance center. (See text for further details.)

Case	Date of genesis at (1200 UTC) (tropical depres- sion stage)	Low-level vorticity (ζ_r) Source at 925 mb ($\times 10^{-5} \text{ s}^{-1}$)	Deep vortex formation	ζ_r at 925 mb	ζ_r at 700 mb	Vertical shear of zonal wind	
				$\left(-\frac{\partial u}{\partial y} \right)$ ($\times 10^{-5} \text{ s}^{-1}$)	$\left(-\frac{\partial u}{\partial y} \right)$ ($\times 10^{-5} \text{ s}^{-1}$)	MLEJ at 700 mb (m s^{-1})	$\left(\frac{\partial u}{\partial p} \right)$ within 700–1000 mb
Hurricane Andrew (1992)	15 Aug 1992 (16 Aug/ 1800 UTC)	Equatorial wave trough	Low- to mid-level easterly wave	3 (2)	3 (2)	18 (wide jet)	-18
TS Ernesto (1994)	19 Sep 1994 (21 Sept/ 1800 UTC)	Monsoon trough	Merger of low- and mid-level vortices	3 (2)	3 (3)	14 (narrow jet)	-8
Hurricane Luis (1995)	27 Aug 1995 (27 Aug/ 1200 UTC)	Thermal vortex/ equatorial wave trough	Merger of low- and mid-level vortices	6 (4)	6 (5)	20 (narrow jet)	-10
Case	PVA at 700 mb ($\times 10^{-10} \text{ s}^{-2}$)	Stretching term $[-\nabla \cdot V(\zeta + f)]$ at 925 mb ($\times 10^{-10} \text{ s}^{-2}$)	Divergence at 925 mb ($\times 10^{-6} \text{ s}^{-1}$)	Saharan air layer depth/width	Potential gradient at 850 mb $\left(\frac{\partial \theta}{\partial y} \right)$ ($\times 10^{-6} \text{ K m}^{-1}$)	Combined barotropic–baroclinic instability $\frac{\partial}{\partial y} \left[(\zeta + f) \frac{\partial \theta}{\partial p} \right] < 0$	Genesis potential $\zeta_{925} - \zeta_{200}$ ($\times 10^{-5} \text{ s}^{-1}$)
Hurricane Andrew (1992)	2	8	-16	(500–850 mb)/ 10°–30°N	10	Not satisfied	0.6
TS Ernesto (1994)	6	16	-28	(600–850 mb)/ 10°–25°N	8	Satisfied	2.4
Hurricane Luis (1995)	6	10	-36	(600–850 mb)/ 10°–25°N	6	Satisfied	4.4

gradient analyses and including additional parameters such as SAL depth/width and genesis potential is presented in Table 1.⁷ The table reveals the following highlights.

- The genesis precursors of all cases occurred 1–2 days prior to their declared tropical depression stage except for the Luis case (parenthetical values in column 2 denote the genesis time obtained from the analyses of this study).
- The low-level vorticity sources (column 3) of these disturbances are either low-level easterly wave disturbances (Andrew), or monsoon trough vortices (Ernesto), or merged vortices from easterly wave disturbances and thermal low pressure systems over the Sahara (Luis).
- Deep vortex formation of all the disturbances result

from the merger of low-level vortices and midlevel vortices (column 4).

- Most of the relative vorticity of the disturbances both at the low and midlevels arises from cyclonic shear of the zonal wind (i.e., the parenthetical values in columns 5 and 6): the midlevel cyclonic shear is provided by the midlevel jet.
- PVA at 700 hPa (column 2 in bottom panel), occurring ahead of the midlevel trough but to the south of the midlevel jet, dominates in two cases (i.e., Ernesto and Luis).
- The low-level stretching (column 3 in the bottom panel) is stronger in Ernesto and Luis than in Andrew, primarily due to stronger low-level convergence (column 4 in the bottom panel).
- Meridional potential temperature gradients pertaining to the SAL (column 6 in the bottom panel), including the associated (MLEJ) vertical wind shears (column 8 in the upper panel), are generally stronger in Andrew than either in Ernesto or Luis due to stronger (i.e., deeper and wider) SAL (column 5 in the bottom panel);
- The combined barotropic–baroclinic instability (column 7 in the bottom panel) criterion over the eastern

⁷ Note that some of the parameters given in the table are maximum values taken within the neighborhood of the genesis location instead of the area-averaged values. This is necessitated by the fact that features such as the MLEJ, horizontal temperature gradient, and vertical shears were located only to the north of the genesis location. However, the genesis parameter is an averaged value over a 5° lat-lon box.

Atlantic appears to be satisfied for the Ernesto and Luis cases (as discussed in the previous section) due to the presence of the SAL to the north of the middle-level jet.

- The daily genesis potential (DGP; column 8 in the bottom panel) is stronger in the Ernesto and Luis cases than in the Andrew case [i.e., Ernesto and Luis possess values greater than the threshold value of 1.6⁸ (and even above the prehurricane depression limit of 1.8), whereas Andrew barely satisfies nondeveloping cluster threshold value of 0.7]. Indeed, the low DGP value for Andrew reaffirms the lack of upper-level support that is necessary for rapid development, as pointed out earlier. Note that persistent upper-level support (through large-scale anticyclonic circulation) appears to be present only in the Ernesto case, in contrast to divergent (convective) outflow associated with the Luis case.

In summary, although all three cases exhibited the presence of the SAL in conjunction with the positive horizontal temperature gradient (indicative of SAL to the north) to the north of the genesis region, only two cases (i.e., Ernesto and Luis) were significantly influenced by the cyclonic shear vorticity on the south side of the middle-level jet. A visual inspection of midlevel (700 hPa) horizontal vorticity advection and low-level (925 hPa) divergence fields for all three cases suggested that there is a general overlap of PVA areas (on the leading and southern edges of the MLEJ, particularly when it is located ahead of the trough axis) with low-level convergence regions in the Ernesto and Luis cases. [These low-level convergence areas appear to be present irrespective of deep moist convection as can be noted from the satellite imagery in the case of Ernesto (see Fig. 4 in Karyampudi et al. 1999).] Therefore, one can argue that the increasing PVA with height up to 700 hPa (since PVA at low levels is negligible) can contribute not only to low-level upward motion (through quasigeostrophic forcing⁹) but more importantly to the occurrence of low-level convergence underneath the PVA from continuity considerations. The concurrent occurrence of larger values of low-level convergence, in conjunction with stronger PVA values in Table 1 in both of these cases than in Andrew, supports the contention that PVA is playing a significant role in increasing the low-level convergence and hence surface cyclogenesis through Sutcliffe's development theorem (Sutcliffe 1947). This implies that a baroclinic mechanism, in general, appears to explain the growth of at least two out of the three cases. The applicability of the baroclinic

mechanism, in turn, is consistent with the satisfaction of the combined barotropic and baroclinic instability for the same two cases as shown in the previous section. However, we find that the original baroclinic mechanism proposed by Karyampudi and Carlson (1988) is inadequate for explaining the deep vortex formation since this study showed that the merger of low- and midlevel vortices dominated the deep vortex formation instead of wave disturbance growth by the CISK mechanism (refer to section 1). Therefore, we propose the following modifications to the baroclinic mechanism.

- An outbreak of a Saharan dust anticyclonic eddy (i.e., the SAL anticyclonic eddy) is favorable for imposing baroclinicity along the leading and southern edges of the SAL front over the eastern Atlantic.
- Cyclonic shear to the south of an elongated midtropospheric jet enhances the midlevel wave trough vorticity, whereas cross- (*vorticity*) contour flow to the south of the jet axis (particularly in the left exit quadrant of the jet) manifests in cyclonic shear vorticity advection on the south side of the jet but downstream of the trough axis.
- The positive vorticity advection, which increases with height below the 700-hPa level, causes wave amplification and enhances low-level convergence to the south and ahead of the jet axis through quasigeostrophic forcing.
- The low-level convergence acts on a preexisting low-level vortex within the monsoon trough to increase the low-level vorticity through vortex stretching. This preexisting low-level vortex, often enhanced by the low-level jet off the North African coast, may have origins either within the heat low over the Sahara ($\sim 20^{\circ}\text{N}$), or from the low-level wave disturbance over the equatorial rainbelt over West Africa ($\sim 10^{\circ}\text{N}$).
- The vertical juxtapositioning of both the low-level vortex and the midlevel vortex associated with the wave trough downstream of the jet leads to the genesis of a tropical depression precursor within the lower troposphere under favorable upper-level forcing.

From Table 1, it is also clear that the SAL depth and width were deeper and wider in the dry year case (i.e., Andrew in 1992) than in the normal year cases (Ernesto in 1994 and Luis in 1995); consequently, the meridional temperature gradient and hence the MLEJ is stronger (and wider) in the dry case. It is known that Saharan dust amounts are heavier in Sahel drought years (Prospero and Nees 1986) and heavy dust concentrations through radiative heating (i.e., aerosol absorption of solar radiation) lead to warmer SAL and hence a stronger and broader jet with less perturbed flow, including a decrease in the convective rainfall in the equatorial region (Karyampudi and Carlson 1988). Furthermore, Grist and Nicholson (2001) have shown that the middle-level jet in dry years is associated with less horizontal shear necessary for instability over the Sahel compared to stronger cyclonic shear to the south of the jet in wet

⁸ This value is given by McBride and Zehr (1981) for pre-hurricane cloud cluster in their Table 1; whereas a value of 1.8 was listed for a pre-hurricane depression.

⁹ Note that quasigeostrophic arguments can be applied since the weekly averaged wind speeds associated with the MLEJ at 700 hPa in all three cases resembled the geostrophic wind speeds at the same level (not shown).

years. *Therefore, the negative influence of the SAL on the genesis of Andrew through a stronger but wider jet along with less perturbed flow and less horizontal shear for (the combined barotropic–baroclinic) instability appear to be consistent with these studies, in contrast to the positive influence of the SAL on the genesis of Ernesto and Luis (in normal Sahel rainfall years).*

These results should be tempered by the fact that the sample size is limited, as mentioned previously, as well as due to the fact that these results were based on a large-scale analysis of the ECMWF data, which appear to contain system phase errors as in the case of Ernesto. Furthermore, these large-scale analyses do not contain mesoscale features such as mesoscale vortices, which may also play an important role in tropical cyclogenesis (e.g., Simpson et al. 1997). However, these processes may be more important in later stages (i.e., tropical depression and tropical storm stages) when the disturbance begins to intensify further than in an early stage of genesis as argued previously. Indeed, these results are consistent with the case study analysis by Molinari et al. (2000) over the eastern Pacific, in which they found that a 700-hPa vortex (located to the south of the midtropospheric jet in conjunction with an easterly wave) merged with a low-level vortex formed within the southwesterly monsoon flow during the genesis of Hurricane Hernan. They claimed that the 700-hPa wave evolved from a background unstable state farther upstream over the Caribbean and the subsequent wave passage controlled all the events involved in the genesis, which is similar to the results presented in this study.

Despite the evidence that large-scale flow conditions control the events in the genesis of tropical cyclones both over the eastern Atlantic and eastern Pacific, it is important to investigate the role of mesoscale vortices in the genesis process in the context of large-scale dynamical influences presented in this study with modeling and observational studies. Since mesoscale observations are not readily available over remote oceanic regions where these systems originate, *in situ* aircraft observations are needed for mapping out the mesoscale details such as the strong horizontal and vertical gradients associated with the MLEJ including the SAL structure, convective vortices etc. to fully understand the multiscale interactions of cyclogenesis. Since Saharan dust outbreaks (i.e., the SAL anticyclonic eddy) propagate farther downstream over the western Atlantic following a leading wave disturbance (Carlson and Prospero 1972), and the SAL is inherently linked to the midtropospheric jet and its dynamics, it is necessary to conduct aircraft investigations (such as with a hurricane reconnaissance aircraft) equipped with an airborne lidar as proposed by Karyampudi et al. (1999). For instance, the existence of a background negative PV gradient maintained by the MLEJ over the western Atlantic region and its role in eastern Pacific cyclogenesis has already been shown by Molinari et al. (2000). However, its role in western Atlantic cyclogenesis as well as the question

of the negative PV anomaly existence to the north of the MLEJ are not well understood, even though we speculate that the negative anomaly is caused by the dust heating within the low static stability air within the dust layer (i.e., the SAL). In addition, in order to fully validate the results from this study, large datasets over longer periods need to be composited to study the genesis mechanisms both in the dry and normal/wet years as well as in contrasting the differences between the systems that develop and those that do not develop over both the eastern and western Atlantic regions.

Acknowledgments. The first author gratefully acknowledges several individuals, who gave inspiration and encouragement over many years to his firm belief that there is a connection between the dust layer and the genesis of tropical cyclones over the Atlantic Ocean. First and foremost is his former advisor, Prof. Toby Carlson, The Pennsylvania State University, who provided the impetus for his interest in African wave disturbances and Saharan dust outbreaks during his graduate student days at Penn State through endless and stimulating discussions that sometimes went beyond normal work hours. Second is Dr. Robert Burpee, the former director of National Hurricane Research Division/AOML/NOAA and NHC/NOAA, whose keen interest and motivation helped to raise his curiosity on the dynamical aspects of dust outbreaks on the growth of wave disturbances. Third is Dr. Richard Reed, whose suggestions to model the African wave disturbances and dust outbreaks have sustained his further interest in their dynamical interactions. Others include Drs. Frank Marks and Peter Black of the Hurricane Research Division (HRD), Miami, Florida, for their trust that there is a connection between the dust layer and tropical cyclogenesis; Dr. Joanne Simpson at NASA Goddard Space Flight Center, Greenbelt, Maryland, for her moral support, encouragement, and inspiration given through her work on vortex mergers in tropical cyclogenesis over the western Pacific; and Dr. Louis Uccellini, Director of NCEP, Camp Springs, Maryland, not only for his conviction that jet dynamics must play an important role in the genesis of tropical cyclones but also for providing moral support in the completion of this work. The authors are also grateful to Sim Aberson of HRD for providing sounding data at a few West African stations for the Ernesto and Andrew cases, as well as to George Lai of GSC/GSFC/NASA, Greenbelt, Maryland, for his help in converting the ECMWF data into GEMPAK format. The first author acknowledges the funding support provided by Ramesh Kakar, program manager at NASA Headquarters through a grant administered by Dr. Dalin Zhang at the University of Maryland, College Park, Maryland, without whose encouragement this work would not have been completed. We also would like to express our appreciation to the anonymous reviewers, whose constructive comments and criticisms greatly helped to refine our presentation.

Much of this work has been performed while the author was affiliated with the Mesoscale Precipitation and Dynamics Branch of NASA Goddard Space Flight Center, Greenbelt, Maryland.

REFERENCES

- Avila, L. A., and E. N. Rappaport, 1996: Atlantic hurricane season of 1994. *Mon. Wea. Rev.*, **124**, 1558–1578.
- Biester, M., and K. A. Emanuel, 1997: The genesis of Hurricane Guillermo: TEXMEX analyses and a modeling study. *Mon. Wea. Rev.*, **125**, 2662–2682.
- Bosart, L. F., and J. A. Bartlo, 1991: Tropical storm formation in a baroclinic environment. *Mon. Wea. Rev.*, **119**, 1979–2013.
- Bracken, W. E., and L. F. Bosart, 2000: The role of synoptic-scale flow during tropical cyclogenesis over the North Atlantic Ocean. *Mon. Wea. Rev.*, **128**, 353–376.
- Briegel, L. M., and W. M. Frank, 1997: Large-scale influences on tropical cyclogenesis in the western North Pacific. *Mon. Wea. Rev.*, **125**, 1397–1413.
- Burpee, R. W., 1972: The origin and structure of easterly waves in the lower troposphere of North Africa. *J. Atmos. Sci.*, **29**, 77–90.
- , 1975: Some features of synoptic-scale waves based on compositing analysis of GATE data. *Mon. Wea. Rev.*, **103**, 921–925.
- Carlson, T. N., 1969a: Synoptic histories of three African disturbances that developed into Atlantic hurricanes. *Mon. Wea. Rev.*, **97**, 256–276.
- , 1969b: Some remarks on African disturbances and their progress over the tropical Atlantic. *Mon. Wea. Rev.*, **97**, 716–726.
- , and J. M. Prospero, 1972: The large-scale movement of Saharan air outbreaks over the northern equatorial Atlantic. *J. Appl. Meteor.*, **11**, 283–297.
- Charney, J. G., and M. E. Stern, 1962: On the stability of internal baroclinic jets in a rotating atmosphere. *J. Atmos. Sci.*, **19**, 159–172.
- desJardins, M. L., and R. A. Peterson, 1983: GEMPAK: An interactive meteorological display and analysis system. Preprints, Ninth Conf. on Aerospace and Aeronautical Meteorology, Omaha, NE, Amer. Meteor. Soc., 55–59.
- Dickinson, M., and J. M. Molinari, 2000: Climatology of sign reversals of the meridional potential vorticity gradient over Africa and Australia. *Mon. Wea. Rev.*, **128**, 3890–3900.
- Douglas, M. W., 1977: The structure and occurrences of disturbances along the ITCZ over the GATE area. Proc. 11th Technical Conf. on Hurricanes and Tropical Meteorology, Miami, FL, Amer. Meteor. Soc., 138–145.
- Emanuel, K. A., 1986: An air-sea interaction theory for tropical cyclones. Part I: Steady-state maintenance. *J. Atmos. Sci.*, **43**, 585–604.
- , 1989: The finite-amplitude nature of tropical cyclogenesis. *J. Atmos. Sci.*, **46**, 3431–3456.
- Farfan, L. M., and J. A. Zehnder, 1997: Orographic influence on the synoptic-scale circulations associated with the genesis of Hurricane Guillermo (1991). *Mon. Wea. Rev.*, **125**, 2683–2698.
- Ferreira, R. N., and W. H. Schubert, 1997: Barotropic aspects of ITCZ breakdown. *Mon. Wea. Rev.*, **125**, 261–285.
- Frank, W. M., 1987: Tropical cyclone formation. *A Global View of Tropical Cyclones*, R. L. Elsberry, Ed., University of Chicago Press, 53–90.
- Gray, W. M., 1968: Global view of the origin of tropical disturbances and storms. *Mon. Wea. Rev.*, **96**, 669–700.
- , 1975: Tropical cyclone genesis. Dept. of Atmospheric Science Paper 323, Colorado State University, Fort Collins, CO, 121 pp.
- , 1998: The formation of tropical cyclones. *Meteor. Atmos. Phys.*, **67**, 37–69.
- Grist, J. P., and S. E. Nicholson, 2001: A study of the dynamic factors influencing the rainfall variability in the West African Sahel. *J. Climate*, **14**, 1337–1359.
- Harr, P. A., R. L. Elsberry, and C. L. Chan, 1996: Transformation of a large monsoon depression to a tropical storm during TCM-93. *Mon. Wea. Rev.*, **124**, 2625–2643.
- Holland, G. J., 1995: Scale interaction in the western Pacific monsoon. *Meteor. Atmos. Phys.*, **56**, 57–79.
- Karyampudi, V. M., 1986: A numerical study of the evolution, structure, and energetics of the Saharan Air Layer. Ph.D. dissertation, The Pennsylvania State University, 287 pp.
- , and T. N. Carlson, 1988: Analysis and numerical simulations of the Saharan air layer and its effect on easterly wave disturbances. *J. Atmos. Sci.*, **45**, 3102–3136.
- , and Coauthors, 1999: Validation of the Saharan dust plume conceptual model using lidar, Meteosat, and ECMWF data. *Bull. Amer. Meteor. Soc.*, **80**, 1045–1075.
- Kurihara, Y., and R. E. Tuleya, 1981: A numerical simulation study on the genesis of a tropical storm. *Mon. Wea. Rev.*, **109**, 1629–1652.
- Landsea, C. W., and W. M. Gray, 1992: The strong association between western Sahelian monsoon rainfall and intense Atlantic hurricanes. *J. Climate*, **5**, 435–453.
- Lau, K.-H., and N.-C. Lau, 1990: Observed structure and propagation characteristics of tropical summertime synoptic scale disturbances. *Mon. Wea. Rev.*, **118**, 1888–1913.
- Lawrence, M. B., B. M. Mayfield, L. A. Avila, R. J. Pasch, and E. N. Rappaport, 1998: Atlantic hurricane season of 1995. *Mon. Wea. Rev.*, **126**, 1124–1151.
- Marks, F. D., Jr., 1980: The origin and development of a tropical mesoscale cloud line. Ph.D. dissertation, Massachusetts Institute of Technology, 145 pp.
- Mayfield, M., L. Avila, and E. N. Rappaport, 1994: Atlantic hurricane season of 1992. *Mon. Wea. Rev.*, **122**, 517–538.
- McBride, J. L., 1981: Observational analysis of tropical cyclone formation. Part I: Basic definition of data sets. *J. Atmos. Sci.*, **38**, 1117–1131.
- , and R. Zehr, 1981: Observational analysis of tropical cyclone formation. Part II: Comparison of non-developing versus developing systems. *J. Atmos. Sci.*, **38**, 1132–1151.
- Molinari, J., D. Vollaro, S. Skubis, and M. Dickinson, 2000: Origins and mechanisms of eastern Pacific tropical cyclogenesis: A case study. *Mon. Wea. Rev.*, **128**, 125–139.
- Montgomery, M. T., and B. F. Farrell, 1993: Tropical cyclone formation. *J. Atmos. Sci.*, **50**, 285–310.
- Norquist, D. C., E. E. Recker, and R. J. Reed, 1977: The energetics of African wave disturbances as observed during Phase III of GATE. *Mon. Wea. Rev.*, **105**, 334–342.
- Prospero, J. M., and T. N. Carlson, 1981: Saharan dust outbreaks over the tropical North Atlantic. *Pure Appl. Geophys.*, **119**, 677–691.
- , and R. T. Nees, 1986: Impact of North African drought and El Niño on mineral dust in the Barbados trade winds. *Nature*, **320**, 735–738.
- Randall, D., T. N. Carlson, and Y. Mintz, 1984: The sensitivity of a general circulation model to Saharan dust heating. *Aerosols and Their Climate Effects*, H. E. Gerber and A. Deepak, Eds., Deepak Publishing, 123–132.
- Reed, R. J., D. C. Norquist, and E. E. Recker, 1977: The structure and properties of African wave disturbances as observed during Phase III of GATE. *Mon. Wea. Rev.*, **105**, 317–333.
- , A. Hollingsworth, W. A. Heckley, and F. Delsol, 1988: An evaluation of the performance of the ECMWF operational system in analyzing and forecasting easterly wave disturbances over Africa and the tropical Atlantic. *Mon. Wea. Rev.*, **116**, 824–865.
- Riehl, H., 1954: *Tropical Meteorology*. McGraw-Hill, 393 pp.
- , 1979: *Climate and Weather in the Tropics*. Academic Press, 611 pp.
- Ritchie, E. A., and G. J. Holland, 1993: On the interaction of tropical cyclone-scale vortices. Part I: Observations. *Quart. J. Roy. Meteor. Soc.*, **119**, 1363–1380.

- Sadler, J. C., 1975: The monsoon circulation and cloudiness over the GATE area. *Mon. Wea. Rev.*, **103**, 369–386.
- Schubert, W. H., P. E. Cieselski, D. E. Stevens, and H.-C. Kuo, 1991: Potential vorticity modelling of the ITCZ and the Hadley circulation. *J. Atmos. Sci.*, **48**, 1493–1500.
- Shapiro, L. J., 1977: Tropical storm formation from easterly waves: A criterion for development. *J. Atmos. Sci.*, **34**, 1007–1021.
- Simpson, J., E. Ritchie, G. J. Holland, J. Halverson, and S. Stewart, 1997: Mesoscale interactions in tropical cyclone genesis. *Mon. Wea. Rev.*, **125**, 2643–2661.
- Simpson, R. H., and H. Riehl, 1981: *The Hurricane and Its Impact*. Louisiana State University Press, 398 pp.
- Spencer, R. W., 1981: A case study of African wave structure and energetics during Atlantic transit. Ph.D. thesis, University of Wisconsin, 103 pp.
- Sutcliffe, R. C., 1947: A contribution to the problem of development. *Quart. J. Roy. Meteor. Soc.*, **73**, 370–383.
- Swap, R., S. Ulanski, M. Cobbett, and M. Garstang, 1996: Temporal and spatial characteristics of Saharan dust outbreaks. *J. Geophys. Res.*, **101**, 4205–4220.
- Thorncroft, C. D., and M. Blackburn, 1999: Maintenance of the African easterly jet. *Quart. J. Roy. Meteor. Soc.*, **125**, 763–786.
- Zehnder, J. A., 1991: The interaction of planetary-scale tropical easterly waves with topography: A mechanism for the initiation of tropical cyclones. *J. Atmos. Sci.*, **48**, 1217–1230.
- Zehr, R. M., 1992: Tropical cyclogenesis in the western North Pacific. NOAA Tech. Rep. NESDIS 61, 181 pp. [Available from National Technical Information Service, 5285 Port Royal Rd., Springfield, VA 22161.]